Modelling shallow landslide locations in Taiwan

Joep Keijsers

Land Dynamics Group

September 2009

WAGENINGEN UNIVERSITY
WAGENINGEN UR

Modelling shallow landslide locations in Taiwan

Joep Keijsers

Master's thesis submitted to Wageningen University in partial fulfilment of the Master of Science degree in Soil Science, specialisation Land Science.

Wageningen, September 2009

Joep Gerardus Servatius Keijsers
joep.keijsers@wur.nl
860814432010

Supervisors

Dr. J.M. Schoorl, Land Dynamics Group
Wageningen University, Netherlands

Prof. Dr. Ir. A. Veldkamp, Land Dynamics Group
Wageningen University, Netherlands

Prof. K.-T. Chang, Department of Geography
National Taiwan University, Taiwan

ACKNOWLEDGEMENTS

Five years of university education and still a lot of help required:

Thanks to my supervisors in The Netherlands: Dr. Jeroen Schoorl for providing the opportunity and giving guidance in this research; Prof. Tom Veldkamp for a lot of insights and valuable suggestions in a short time.

Thanks to helpful people in Taiwan: Prof. Karl Chang for supplying me with data, arranging fieldwork logistics and giving useful suggestions; Gilbert and Thomas for your help and discussions; Prof. Hongey Chen and students in the Geosciences lab for their advice and assistance in the laboratory measurements.

Thanks to my fellow student Jasper for sharing scientific thoughts, being invaluable company and waking me in the mornings.

ABSTRACT

Landslides pose important threats to ecosystems, constructions and human life. The physically-based shallow landslide model LAPSUS-LS is tested for its performance in predicting shallow landslide locations induced by a typhoon in a mountainous catchment in northern Taiwan. After calibration, the best model performance is achieved with parameter values that differ significantly from field measurements, mainly because of scaling effects and model abstractions. Incorporating the spatial distribution of rainfall and optimising the performance per land use type both improve the predictions, although the maximum performance is mostly limited by model abstractions and resolution. The model performance decreases at coarser resolutions because of topographical smoothing. At the 27 m resolution used in this study, 75% of the landslides are predicted and 80% of the stable cells are correctly predicted. With limited data and simple equations, the model is able to predict the spatial pattern of actual landslides and show the effects of changes in parameters or scenarios.

Keywords: landslide locations, physically-based model, land use, model resolution, LAPSUS, model performance, Taiwan

TABLE OF CONTENTS

1 INTRODUCTION

Strong uplift, frequent earthquakes and typhoons and rapid weathering create a mountainous environment in which shallow landsliding is the dominant mass wasting process (Chang, 1986; Hovius et al., 2000; Dadson et al., 2003). The erosion and subsequent deposition of hillslope material can lead to sedimentation of rivers and reservoirs, loss of soil fertility, disturbance of ecosystems and poses a threat to constructions and human life. Most landslide studies therefore are aimed at mapping landslide hazards for regional and urban planning (e.g. Mejía-Navarro, 1994; Van Beek and Van Asch, 2004; Keim and Skaugset, 2003; Anbalagan et al., 2008; Claessens et al., 2007b; Baum et al., 2005), offering useful tools and insights to decision makers in land use planning.

Based on steady-state hydrology assumptions and the infinite slope stability model, several landslide hazard prediction models have been developed (e.g. Montgomery and Dietrich, 1994; Wu and Sidle, 1995; Burton and Bathurst, 1998; Borga et al., 2002; Claessens et al., 2007a). In this research, LAPSUS-LS is used to model shallow landsliding in a 120 km^2 mountainous catchment in Northern Taiwan. The model is based on the LAPSUS framework (Schoorl et al., 2000) and a landslide module (LS) has been added (Claessens et al., 2007a). The model is able to predict landslide initiation and subsequently estimates the landslide path and volume and adapts the elevation data accordingly. LAPSUS-LS is developed to address the on and off-site effects of shallow landslides to provide insights in the landscape evolution on the time scale of years to decades on a catchment scale. For timescales over multiple years, temporal dynamics become important. Landslide locations of previous years influence the locations of next years, not only through changes in the elevation, but also because of the removal of possible landslide material. To incorporate this so called legacy effect in the model, rates of weathering, uplift, river incision and soil redistribution have to be quantified.

Because little is known about these factors, in this study LAPSUS-LS is optimised for a single event. The event that is considered is 2004 typhoon Aere, whose intense rainfall caused numerous landslides. By changing the values of three model parameters, the model prediction of landslide locations rather than sediment volumes is optimised.

Because intense rainfall associated with typhoons is an important shallow landslide trigger and its spatial distribution can be highly variable, incorporation of this distribution can be important in determining landslide locations (Chiang and Chang, 2009). Therefore, a rainfall map is derived from radar images and incorporated in the model, to see the effect on model performance.

Another important factor determining landslide risk is the land use. It is generally accepted that vegetation has a positive influence on slope stability, although negative contributions are also present (Sidle et al., 1985; Greenway, 1987). For vegetation, the most important mechanical controls on slope stability are root reinforcement and root anchoring, while evapotranspiration, rainfall interception and increased infiltration are the most significant contributions to changing the slope hydrology (Greenway, 1987). To account for possible influence of these effects, the model performance is optimised separately for the dominant land use types in a recent land use map. A theoretical land use change scenario is then applied and the resulting changes in landslide susceptibility are studied. Finally, the study compares the model's performance at

different modelling resolutions in order to understand the limitations the modelling resolution poses.

The results of this research will give insight in the ability of the LAPSUS-LS model to predict landslide locations for a single event at different modelling resolutions. It will shed light on the value of a rainfall map and on the effect of land use stratification on the model performance. Finally, some recommendations for future research are made.

2 MATERIALS AND METHODS

2.1 STUDY AREA

Taiwan and its mountain range originate from the ongoing collision between the Eurasian and Philippine Sea plates, resulting in strong uplift and frequent earthquakes. Estimated recent uplift rates range from 2 to 8 mm/y, with strongest uplift in the centre of the island (Chen and Liu, 2000; Liew et al., 1993). Taiwan has a sub-tropical climate and monthly average temperatures range from 15°C in January to 29 °C in July. Approximately half of the annual precipitation sum of 2325 mm occurs during the June-September typhoon season (CWB, 2009). Because of the steep topography, high intensity typhoons and frequent earthquakes, landslides are a recurrent phenomenon.

The Shihmen catchment is located in the north-western part of the central mountain range. It drains into the Shihmen reservoir, the largest multi-purpose water reservoir in northern Taiwan and therefore the catchment is frequently monitored and has more data available than other mountainous catchments (Chang and Chiang, 2008). The south part of the Shihmen catchment is taken as the study area for this thesis. The eastern part (120 km^2) is used for calibration, the western part (196 km^2) for validation (Figure 1). The elevation ranges from 825 m to 3375 m in the calibration area and from 825 m to 3470 m in the validation area, while having an average slope angle of 33° and 35° respectively. In both cases, slopes become steeper near the streams and this is also where landslide density is the highest (Figure 2).

Tertiary slate, shale, phyllite and sandstone are the dominant lithologies and are mostly covered by shallow soils with little soil formation. However, there are also small areas with thick layers of unconsolidated material. 78% of the calibration area is covered with broad-leaf forest, 14% with needle-leaf forest and the remaining 8% consist of agricultural patches, built-up areas and bamboo forest. For the validation area these numbers are 53%, 44% and 3% respectively.

2.2 TYPHOON AERE

The event that will be simulated and studied in this research is the 2004 typhoon Aere. This event is chosen because of:

- the availability of a landslide inventory map specifically dedicated to the event;
- availability of radar data for estimation of spatial rainfall distribution in between rain gauges;
- the intensity of the event, decreasing influences of smaller events that occurred just before or after Aere;

After growing from a tropical depression to a typhoon above the Pacific Ocean, Aere struck the north of Taiwan from August 23th to 25th. The total precipitation measured in the calibration catchment in these days is 1607 mm, with a maximum of 960 mm on August 24th. It is the highest amount of daily rainfall registered at the Baichi rain station since 1982 at least. The total area of landslides generated or reactivated in the calibration catchment is 267 ha, or 2% of its

total area, for the validation catchment this is 212 ha, or 1% of its total area with average landslide sizes 0.63 ha and 0.40 ha respectively.

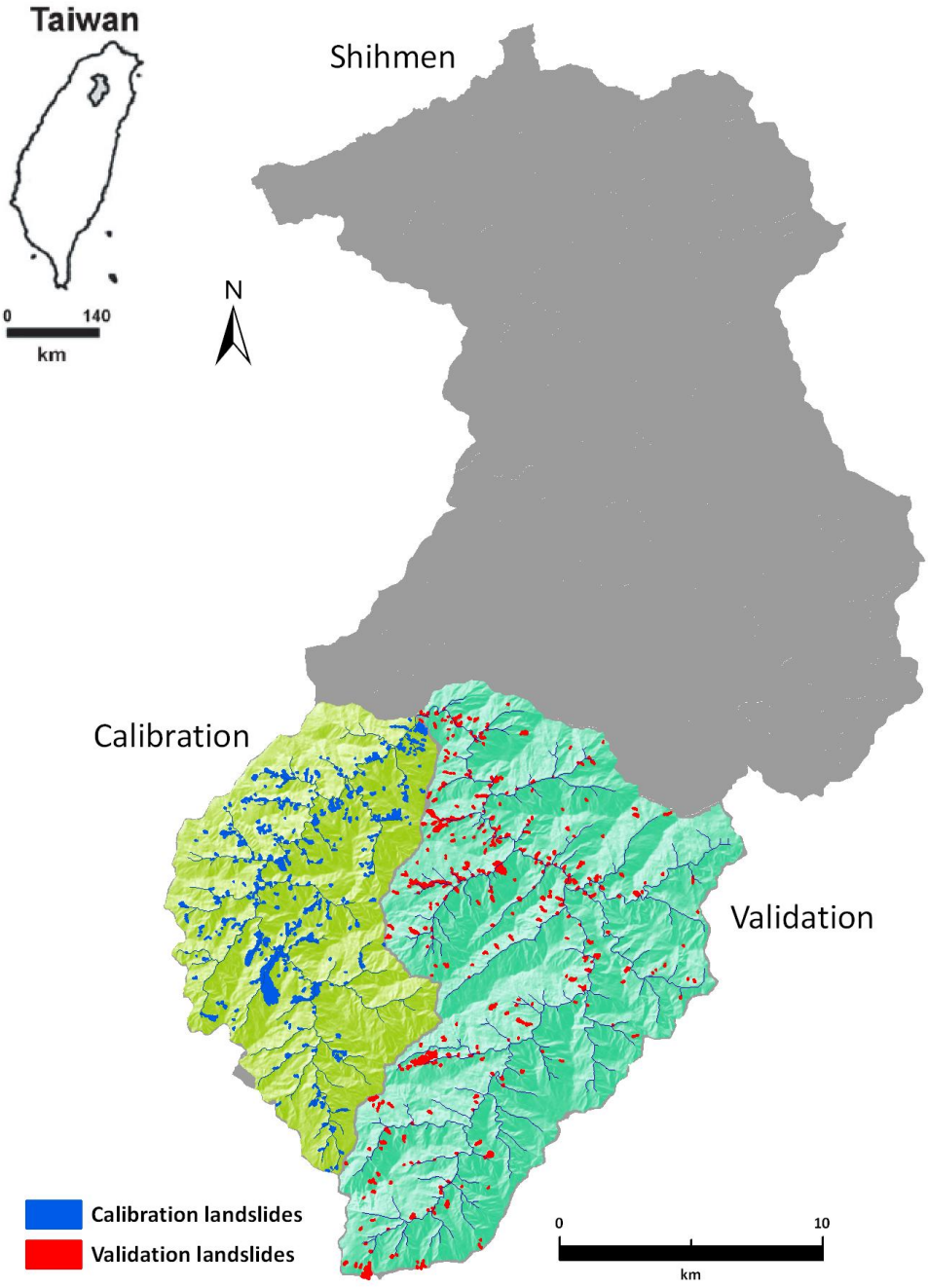

Figure 1. Location of the Shihmen catchment in Taiwan and the study area within Shihmen. Landslides associated with Aere are shown for both calibration and validation.

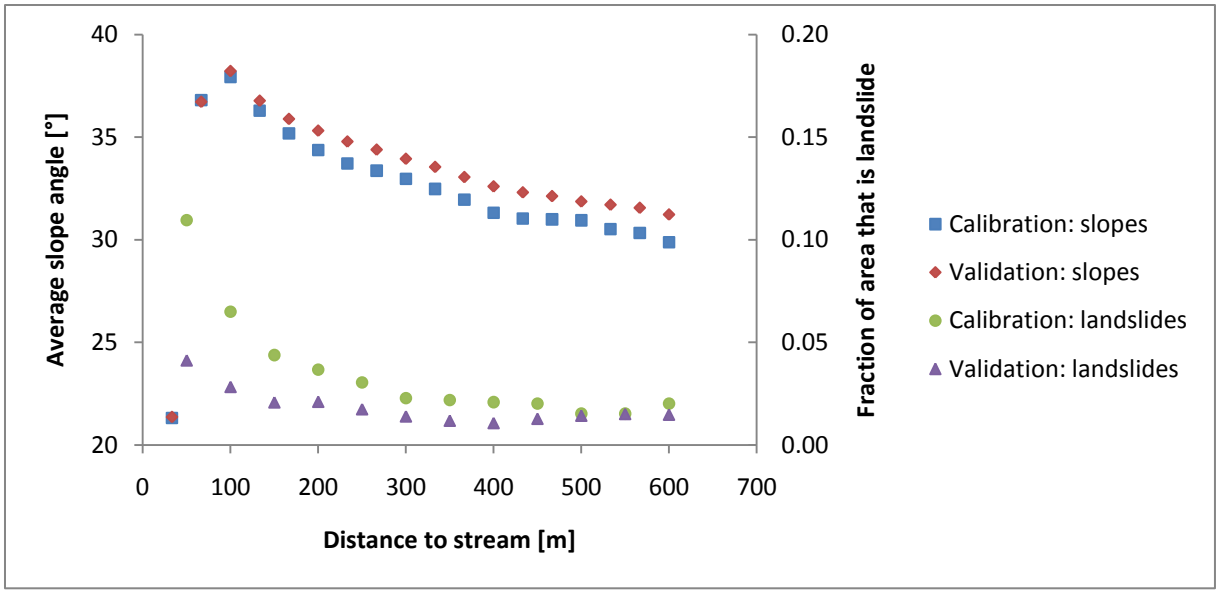

Figure 2. Average slope angle and fraction of area that is covered by landslides at different distances from the river.

2.3 MODELLING FRAMEWORK

In this thesis the LAPSUS (LandscApe ProcesS modeling at mUlti dimensions and scales; modelling framework is used, which is a three-dimensional landscape evolution model, addressing on-site and off-site effects of current and possible water and soil redistribution by water run-off and tillage erosion (Schoorl et al., 2000). A landslide component was added to the LAPSUS framework by Claessens et al. (2007a), called LAPSUS-LandSlide (LAPSUS-LS), which is able to model the triggering of shallow landslides and their subsequent movement downslope. First the amount of rain that will trigger a landslide (the critical rainfall, Q_{cr}) is calculated on a cell basis in a grid structure. Then, after a landslide is triggered in a certain rainfall scenario, the downslope trajectory is calculated for both the erosion and deposition phases of the landslide.

2.3.1 CALCULATION OF CRITICAL RAINFALL

The calculation of critical rainfall is based on previous work by Montgomery and Dietrich (1994) and Pack et al. (2001) where a steady state hydrologic model is combined with a deterministic infinite slope stability model to delineate areas prone to landsliding due to surface topographic effects on hydrologic response (Claessens et al., 2007a). In an infinite slope stability model the stability of a slope is usually expressed as the factor of safety (FS), which is defined as (Selby, 1993):

$$FS = \frac{sum\ of\ resisting\ \ forces}{sum\ of\ driving\ \ forces} \qquad (1)$$

The sum of resisting forces consists of all forces that resist slope failure; the sum of driving forces consists of all forces that act in favour of slope failure. If FS is larger than 1 the slope is stable, if FS is below 1, the slope becomes unstable and a landslide will start at that position. FS can be written as (Pack et al., 2001; Claessens et al., 2007a):

$$FS = \frac{C + \cos\theta\left[1 - W\left(\frac{\rho_w}{\rho_s}\right)\right]tan\varphi}{sin\theta} \quad (2)$$

With C combined cohesion [-], θ local slope angle [°], W a relative wetness index [-], ρ_w the density of water [g cm^{-3}], ρ_s the wet soil bulk density [g cm^{-3}] and ϕ the effective angle of internal friction of the soil [°]. The combined cohesion can be interpreted as the relative contribution to slope stability of the cohesive forces, which consist of root cohesion and soil cohesion. It is made dimensionless relative to the perpendicular regolith thickness as defined in Claessens et al. (2007a):

$$C = \frac{c_r + c_s}{h\rho_s g} \quad (3)$$

where c_r is root cohesion [N m^{-2}], c_s is soil cohesion [N m^{-2}], h is regolith thickness perpendicular to the slope [m] and g is the gravitational acceleration constant [m s^{-2}]. W (relative wetness) is the ratio of local flux at a given steady state rainfall to that at soil profile situation. A steady state hydrologic response model based on the work by O'Loughlin (1986) and Moore et al. (1988) as cited by Claessens et al. (2006) is used for the calculation of W:

$$W = \frac{Ra}{bTsin\theta} \quad (4)$$

With R steady state rainfall recharge [m day^{-1}], a the upslope contributing drainage area [m^2], b the grid size [m], T horizontal transmissivity when saturated [m^2 day^{-1}] and θ the local slope angle [°]. The upslope contributing area is calculated using the concept of multiple downslope flow (Quinn et al., 1991).

Wetness ranges between 0 and 1, since any excess of water is assumed to form overland flow. If equation

4 is substituted in equation 2; the minimum steady state rainfall predicted to cause slope failure can be determined by setting FS at 1 (the threshold for instability) and solving for R. This amount is called the critical rainfall (Q_{cr}) and can be written as follows (Claessens et al., 2007a):

$$Q_{cr} = Tsin\theta\left(\frac{b}{a}\right)\left(\frac{\rho_s}{\rho_w}\right)\left[1 - \frac{sin\theta - C}{cos\theta tan\varphi}\right] \quad (5)$$

with the boundary condition for W (between 0 and 1), the upper and lower thresholds for slopes that can fail according to equation (6) can be calculated. Unconditionally stable areas are always predicted to be stable, even when saturated and satisfy the following condition (Claessens et al., 2007a):

$$tan\theta \leq \left(\frac{C}{cos\theta}\right) + \left(1 - \frac{\rho_w}{\rho_s}\right)tan\varphi \quad (6)$$

Unconditionally unstable areas, consisting mostly of bedrock outcrops, are unstable even when dry and satisfy the following condition (Claessens et al., 2007a):

$$tan\theta > tan\varphi + \left(\frac{C}{cos\theta}\right) \quad (7)$$

2.3.2 *TRAJECTORIES OF FAILED SLOPE MATERIAL*

Landslides start at grid cells when the amount of rainfall applied to the cell exceeds the critical rainfall calculated for that cell. The landslide then moves downslope using a steepest descent algorithm. The amount of material S [m] which is eroded in each cell that the landslide moves through is calculated in the following equation (Claessens et al., 2007a) and is limited by the regolith depth h at each cell:

$$\text{if } \frac{\rho_s cos\theta\,(tan\theta - tan\alpha\,)a}{c_s} \leq h \rightarrow S = \frac{\rho_s cos\theta\,(tan\theta - tan\alpha\,)a}{c_s}$$

$$\text{if } \frac{\rho_s cos\theta\,(tan\theta - tan\alpha\,)a}{c_s} > h \rightarrow S = h \qquad (8)$$

with ρ_s the saturated bulk density [g cm^{-3}], θ the local slope angle [°], α the rest angle at which the erosion phase stops and deposition starts [°], c_s the soil cohesion [N m^{-2}] and a a correction factor for dimensions [m^2]. The run-out distance r [m] of the depositional phase is calculated using the following equation from Burton and Bathurst (1998):

$$r = \Delta y \cdot f \qquad (9)$$

where Δy [m] is the elevation difference between the initiation point of the landslide and the point at which deposition begins and f is an empirical derived fraction. The number of downslope grid cells involved in the deposition of landslide material is defined as 'cell-distance' D [-] and is calculated as (Claessens et al., 2007a):

$$D = \frac{r}{b} \qquad (10)$$

where r is the run-out distance [m] and b is cell size [m]. The accumulated material is then further routed with 'double' multiple flow methodology to downslope neighbours until $D < 1$, when all the remaining sediment is deposited and the landslide halts (Claessens et al., 2007a).

2.4 INPUT DATA

2.4.1 *FIELDWORK*

Regolith depth (h)

The thickness of the layer of loose material (regolith) on top of the bedrock has been measured, assuming that this is the maximum depth of a possible shallow landslide. Measurements were taken at 56 sites in the Baichi catchment, either by observing road cuts or other exposed profiles or by hammering a metal pin of 1.70 m length into the regolith until the assumed bedrock was hit. At every site, several measurements were made to account for small scale variability. In some cases, a soil pit was dug next to the pin measurement to ascertain that the pin had hit bedrock. One important problem is that regolith depths over 1.70 m could not be measured with the described method. In those cases, regolith depth was noted as *at least* the measured depth. Another problem arises because of the general high stoniness of the soils in the catchment: a large loose block will give the same measurement feedback as solid bedrock.

Bulk density (ρ_s)

For determination of saturated bulk density 9 sites have been sampled in two different parent materials and different land use types. Saturated bulk density is difficult to measure directly in the field, so it has been calculated from the dry bulk density and pore space. Large samples were

taken, to reduce the influence of possible edge effects and small measurement errors and to include the omnipresent rock fragments in the measurement.

The sampling was done using a metal tube with an inner diameter of 40 cm. After removing the organic litter layer and inserting the tube into the ground to a known depth, the contained volume of soil was extracted and taken to the lab for analysis. The samples were dried overnight at 110°C. Next, the samples were sieved to separate the coarse fraction (>2mm) from the fine earth fraction (<2mm) and both fractions were then weighed separately.

To determine pore space, which in case of saturation would be filled with water, the total sampled volume was calculated from the tube diameter and depth of insertion. By using a water filled container with volume indications, the volume of all particles was determined by the water displacement caused by adding the particles to the container. The total volume of the sample minus the volume of all particles equals the soil pore space. Stoniness was calculated as fraction of coarse materials to the total sampled volume. By multiplying the pore space with the bulk density of water and adding it to the weight of the particles, the saturated bulk density was calculated.

Soil cohesion and angle of internal friction (c_s and φ)

Soil cohesion and angle of internal friction were measured in a direct shear test. In such a test the dry shear strength is measured by putting a dry soil sample in a direct shear test machine and moving the top and bottom half of the sample horizontally in opposite directions while having a fixed normal stress (*normal* in this case refers to the direction of the force) from above. This stress is the result of a weight on top of the soil sample. The maximum pressure that develops horizontally before the top and bottom half shift relative to each other (failure) is the shear strength of the soil. The general idea is that the resistance of the soil to failure is higher at higher normal stresses. Shear strength is related to normal stress (according to Coulomb's law as stated in e.g. Head (1994)):

$$\tau = c_s + \sigma_n \cdot \tan\varphi \tag{11}$$

where τ is shear strength [kPa], c_s is soil cohesion [kPa], σ_n is normal stress [kPa] and φ is the angle of internal friction [rad]. If multiple samples are tested with different normal stresses, a line can be plotted relating dry shear strength to normal stress. The slope angle of this line is the angle of internal friction, the intercept is the soil cohesion.

However, LAPSUS-LS needs the soil cohesion and angle of internal friction under saturated conditions. To measure saturated shear strength, a tri-axial test should be done on a saturated sample, however this was not possible in the time span of this research. Saturated shear strength can also be approximated by converting dry normal stress (σ_n) to effective normal stress ($\sigma_n^{'}$), as done in the following formula:

$$\tau = c_s^{'} + (\sigma_n - u) \cdot \tan\varphi^{'} = c_s^{'} + \sigma_n^{'} \cdot \tan\varphi^{'} \tag{12}$$

Where $c_s^{'}$ is effective soil cohesion [kPa], u is pore water pressure [kPa] φ' is the effective angle of internal friction [rad] and $\sigma_n^{'}$ is effective normal stress [kPa] (Head, 1994; Selby, 1993). Pore pressure u can be calculated as follows:

$$u = \frac{\rho_w \cdot z \cdot g \cdot w}{1000} \quad (13)$$

Where ρ_w is the density of water [kg m^{-3}], z is the depth in the soil at which the shear test sample is located [m], g is the gravitational acceleration constant [9.81 m s^{-2}] and w is the water content of the soil [-], 1 meaning fully saturated and 0 meaning completely dry. The factor 1000 is needed to correct for the different units. Since the depth z is simulated by putting a specific normal stress on top of the sample (representing the weight of the above lying soil column), z can be calculated as follows:

$$z = \frac{\sigma_n \cdot 1000}{\rho_s \cdot g} \quad (14)$$

With ρ_s wet soil bulk density [kg m^{-3}]. The factor 1000 is needed to correct for the different units.

At test conditions, $w = 0$, consequently $u = 0$ (equation 13), and in that case the effective normal stress (σ'_n) equals the regular normal stress measured at w = 0 (σ_{n0}):

$$\sigma'_n = \sigma_n - u = \sigma_{n0} \quad (15)$$

The required saturated conditions can be simulated by calculating the pore pressure for $w = 1$. The effective normal stress σ'_n for w = 1 (now named saturated normal stress σ_s) can be calculated from the measured dry normal stress (σ_{n0}) using the following formula:

$$\sigma_s = \sigma_{n0} + u \quad (16)$$

and the resulting shear strength for saturated soil (τ_s):

$$\tau_s = c'_s + (\sigma_{n0} + u) \cdot \tan\phi' = c'_s + \sigma_s \cdot \tan\varphi' \quad (17)$$

When the simulated saturated normal stress and measured shear strength are drawn in a graph, the soil cohesion and angle of internal friction under saturated conditions can be calculated.

Samples from three locations with different land uses in the study area were used. These samples were first dried overnight at 110°C and then sieved with a 2 mm sieve to separate the coarse from the fine fraction, since the direct shear test machine can only handle samples without rock fragments. The test equipment was calibrated according to ASTM (2004). For each test the sample ring was filled with new material. Every sample was tested with a normal pressure of 17.35, 34.70, 69.39 and 138.78 kPa (corresponding to weights of 5, 10, 20 and 40 kg). One sample was tested three times with all normal pressures to make sure that the instrument gave consistent results.

Minimum angle for maintaining flow (α)

The minimum angle for maintaining flow α is measured in fieldwork and derived in a GIS as the average minimum slope angle for landslides in the calibration catchment. The mean of minimum slope angle for the 2004 landslides on the 27m DEM is 28°. Field measurements of original slope angles at debris depositions in the catchment give 27°, but these were small scale depositions, probably without representative momentum. As initial value, 27° is used.

2.4.2 LITERATURE

Transmissivity value T in $m^2\ d^{-1}$ has been taken from Chang and Chiang (2009). The average of three geological units (75 $m^2\ d^{-1}$) is used for the entire catchment, as the three geological units all comprise similar lithologies. The empirical run-out length f is taken from Burton and Bathurst (1998) and equals 0.4. In literature, root cohesion (c_r) values have been determined for different vegetation types in different climates. Greenway et al. (1987) found root cohesion of 3 kPa representative for a broad-leaf hillslope forest in Hong-Kong. As all involved parameters are known, combined cohesion can now be calculated with equation 3.

2.4.3 MAP PREPARATION

DEM

A 27 m DEM is used in this study, which is aggregated from 9 m cell size for two reasons. First, it significantly reduces computation time in LAPSUS-LS. Second, the DEM has dubious artefacts: the gradient (especially in the rivers) is not constant, but consists of staircase-like sequence of flats and sudden drops, and other staircase profiles are present on the slopes as well. Aggregating the DEM to 27 m has a smoothing effect, whereby the flats and sudden drops are much less profound. The sinks in this DEM are filled after which all flats and pseudo-flats are removed, which is needed for LAPSUS-LS to work correctly. The catchments are defined as all cells that drain towards the confluence of the rivers draining both catchments.

To investigate the influence of the modelling resolution on model performance, DEMs of 54 m and 81 m have been aggregated from the 9 m DEM.

Landslide map

For calibration, the landslide inventory map of the 2004 air photo is used (Figure 1). It contains all active landslides of 2004 and does not distinguish between erosion part and deposition part. Because the simulated event (Aere) has the highest intensity, it is assumed that all active landslides in the inventory map can be related to the Aere event. The inventory map has been clipped to the calibration catchment's extent. Landslide polygons with an area smaller than a square 27 m cell have been removed, because these are considered too small to be represented by the modelling resolution. For the remaining landslide polygons, a buffer of a half cell size has been applied to avoid losing landslide area in discretisation. Finally, the landslide map is converted to a 27 m raster for the model.

For the validation catchment, a landslide inventory map of 2005 is used as basis (Figure 1). The map is visually compared with a 2004 air photo. Because little is known about the origin of this map, it could have a different producer and hence a different production method. As demonstrated by Ardizzone et al. (2002), the detail and precision of a landslide inventory is primarily dependent on the producer's skill and experience. This could cause a discrepancy between the map used for validation and the map used for calibration.

Land use map

Land use can have significant influence on the stability of slopes. Management practices and vegetation can influence the hydrology and the cohesion of the soil. It is well known that vegetation can stabilise the soil and reduce the landslide risk (Sidle et al., 1985; Greenway, 1987).

To incorporate these effects of land use, a 2005 land use map of the Shihmen catchment is used for stratification. The 5 dominant land use types are extracted and merged together. Built-up areas and roads were left out, because the modelling resolution is not adequate for correct representation of e.g. buildings and roads. Blank spaces that result of smaller disregarded land use types were assigned the land use type of the surrounding cells.

The resulting land use classes are: broad-leaf forest, needle-leaf forest, bamboo patches, arrow bamboo forest and agricultural fields. After reclassifying the field observations to the same land use classes, the Shihmen land use map has a 72% overall agreement with the 79 observation points.

Rainfall map

To incorporate the spatial distribution of rainfall in the area, a maximum 24 hour rainfall intensity map derived from radar reflectivity data is incorporated in the model.

As done by Chiang and Chang (2009), 10-minute radar reflectivity data at 1 km resolution from the QPESUMS radar network spanning Taiwan were obtained. The 10-minute data of the Aere typhoon were averaged to hourly values and, using a conversion developed by the Central Weather Bureau of Taiwan, converted into rainfall rates. The rainfall rates were then calibrated to match the rain stations in and just around the calibration and validation catchment of this study. The maximum 24 hour precipitation (in mm h^{-1}) was then derived for every 1 km cell. The resulting map is resampled to 27 m using bilinear interpolation and cut to the catchment extents for model use. Correlation between radar derived rainfall intensities and ground based stations for a catchment in Central Taiwan is found to be 0.9 (Chen et al., 2007).

2.5 CALCULATION OF MODEL PERFORMANCE

For calibration, it is convenient to have one value that indicates the goodness of prediction of both unstable and stable cells. If only the prediction of landslide cells is accounted for, an entire catchment of landslide cells would lead to a perfect classification, not accounting for the misclassification of actual stable cells. By incorporating the correctly predicted stable cells as well, over-prediction of unstable cells decreases the performance. Furthermore, the calculation of model performance should not be sensitive to prevalence, which is the unequal sample sizes of negative and positive cases, in this case stable and unstable cells. This can be accounted for by calculating the proportion of positive and negative cases that are successfully predicted separately, instead of using the proportion of total cells that is correctly predicted (either stable or unstable) to the total number of cells (Beguería, 2006).

As suggested by Huang and Kao (2006), the Modified Success Rate (MSR) is used. This is a linear combination of the fraction of landslides that are correctly predicted (on a polygon basis) and the producer's accuracy of stable cells (on a cell basis). Landslide prediction is calculated per polygon, because one small failure often leads to an increasingly large area of failure. Subsequent upslope failure may be triggered as the ground slope of the upslope soil mass is effectively increased by the removal of the support provided by the initially failed material. Subsequent downslope failure may occur as the initially failed material is mobilized as a debris flow and adds to the weight of downslope positions (Reneau and Dietrich, 1987, in: Burton and Bathurst, 1998)

A landslide polygon is counted as correctly predicted if one or more cells with predicted erosion occur within its boundary. A stable cell is considered correctly predicted if it is a cell without erosion or deposition and is not contained in a mapped landslide polygon. Because the hand drawn landslide polygons are never extended into the streambed, whereas in reality they often deposit sediments in the streambed, the amount of incorrect sedimentation cells is overestimated. This causes a decrease in the number of correctly predicted stable cells, resulting in a slightly lower performance.

MSR can be calculated as follows:

$$MSR = 0.5 \times \frac{a}{b} + 0.5 \times \frac{c}{d} \tag{18}$$

In which:

a : number of landslide polygons that are correctly predicted
b : total number of landslide polygons
c : number of stable cells correctly predicted
d : total number of actual stable cells

MSR can range from 0 to 1, predicting all cells as stable or all cells as landslide yields 0.5. Best score is achieved when both the landslide polygons and stable cells are perfectly predicted, leading to a score of 1. The calculation of MSR is implemented in the LAPSUS-LS model for automatic calculation.

2.6 CALIBRATION AND VALIDATION PROCEDURE

The prediction of landslide locations by the LAPSUS-LS model is optimised for the 2004 typhoon event Aere in the southern part of the Shihmen catchment. Although field measurements give realistic parameter values and all parameters have a physical meaning, calibration is necessary because point measurements are not necessarily the best representation for a grid cell average. For calibration the western sub-catchment is used, for validation the eastern catchment (Figure 1). The results considered for optimisation are the correct prediction of both landslide and stable cells compared to a landslide inventory map, compiled for the specific event.

The Modified Success Rate (MSR) is used as measure for model performance, and is calculated using the number of correctly predicted landslide polygons and the number of correctly predicted stable cells. The higher the MSR, the better the all-round model performance.

To understand the separate effects of changes in model parameters or the addition of extra information to the model, the calibration is done in 3 steps.

In the first step, the model is tested using the input parameters derived from fieldwork and literature and the resulting model performance is calculated. For rainfall, the maximum rainfall measured in the catchment's rain station is used for the entire catchment, disregarding spatial distribution of rainfall.

In the second step, the model performance is optimised by adapting the model parameters. Apart from the local slope angle θ and wetness *W*, all cells have the same parameter values. The amount of rainfall *R* and the transmissivity *T* are lumped to the hydrological parameter *R/T*. As both are linked linearly in the model, this limits the amount of possible parameter combinations as only their ratio is used. The input values range from 0.001 m^{-1} to 0.01 m^{-1} with 0.0001 m^{-1} increments. Next input parameter is the dimensionless combined cohesion *C*, which aggregates c_r, c_s, ρ_s and *h* into one factor by equation 3. Input ranges from 0.1 to 1.0, with 0.01 increments. The last parameter for calibration is angle of internal friction φ, for which the range of 29.4° to 40.4° with 0.5° steps is applied.

Step 3 is the addition of information to the model. First, the influence of the spatial distribution of rainfall is incorporated separately. The spatial distribution of the maximum 24 hour rainfall intensity in the area has been derived from radar images (Chiang and Chang, 2009) and is introduced into the model as a rainfall coefficient. The model is then optimised by changing *C* and *R/T*.

Next, the effect of land cover or land use is considered by stratifying the area according to five dominant land use units on a land use map, being broad-leaf forest, needle-leaf forest, arrow bamboo forest, bamboo patches and agricultural fields. Land use can have significant influence on the stability of slopes, most importantly by adding root reinforcement and changing the hydrology. It is well known that trees can stabilise the soil and reduce the landslide risk (Sidle et al., 1985; Greenway, 1987). In the model, the influence of vegetation on cohesion will be accounted for by adapting *C*, the influence of land use on hydrology will be accounted for by adapting *R/T*, both within the same ranges as applied in step 2.

For validation, the parameter values from the runs with the highest MSR are used as input for the validation catchment and the performance of LAPSUS-LS in the validation catchment will be calculated.

To investigate the influence of the DEM resolution on the model performance, the step 2 model calibration as described above is done as well for the original 9 m DEM, a 54 m DEM and 81 m DEM, both aggregated from the original 9 m DEM.

2.7 APPLICATION PROCEDURE

Land use changes can have profound effects on the hydrology and stability of a slope (e.g. Van Beek and Van Asch, 2004, Hong et al., 2009, Bathurst et al., 2009).

To demonstrate a practical use of the model and its calibration per land use type, a simple theoretical land use change scenario is created and the influence of the land use change on the occurrence of shallow landslides is investigated.

The theoretical scenario represents the clearing of forests surrounding agricultural fields and built-up areas and turning it into agricultural fields. This might be done to increase the size of agricultural fields or to allow expansion of settlements. A 100 m buffer into natural forests is applied to agricultural fields and built-up areas. Because no realistic calibrated value is found for agricultural fields, the combined cohesion *C* cannot be set at the value for agricultural fields. Therefore, combined cohesion is assumed to decline because of a decrease in root cohesion c_r.

The initial decline in root cohesion after harvest in broad-leaf forest is estimated at 50% (Sakals and Sidle, 2004). After halving the root cohesion of broad-leaf forests and keeping the other factors of equation 3 constant, the combined cohesion for the cleared areas is set at 0.15.

The adapted land use map for the calibration catchment is loaded into the model and, with the values calibrated in step 3 for the original land use map, the effects of a theoretical land use change scenario on shallow landsliding are considered. This implies that an event with the same intensity as Aere is used to trigger landslides under the changed land use conditions.

3 RESULTS AND DISCUSSION

3.1 FIELDWORK RESULTS

3.1.1 BULK DENSITY

Samples from 9 different sites have been analysed for saturated bulk density, porosity and stoniness. No relation between saturated bulk density and land use or geology could be found, so the average value is used for both the calibration and validation catchment. Resulting values are listed in Table 1. The average value is in good correspondence with the saturated bulk density based on 15 samples by Braakhekke (2007) (1.58-1.78 g cm^{-3}) and is slightly lower than the values used in Chang and Chiang (2009), ranging from 1.72 to 1.82 g cm^{-3}.

Table 1. Bulk density results

	porosity [-]	stoniness [-]	saturated bulk density [g/cm3]
average	0.50	0.36	1.66
st. dev.	0.08	0.07	0.12

3.1.2 REGOLITH DEPTH

Regolith depth measurements were taken at 56 sites and the results are plotted against the slope angle (Figure 3). At each slope angle class there is a large range of possible regolith depths, even at short distances. This is also reported by Uchida et al. (2008) for the Japanese mountain range and by Bathurst et al. (1998) for Scotland. The regolith depth is often dependent on the geomorphology, but in this research, no satisfactory relation between slope curvature, slope angle and depth of the regolith is found. The measured depth of shallow landslides is mostly between 0.5 - 2 m, (Braakhekke, 2007; Chen and Wu, 2007), which is in the range of regolith depths found for slope angles from 30° to 60° (Figure 3). Therefore, a uniform regolith depth of 1 m is assumed for the study area. This corresponds with the value used for the same catchment in Chang and Chiang (2009).

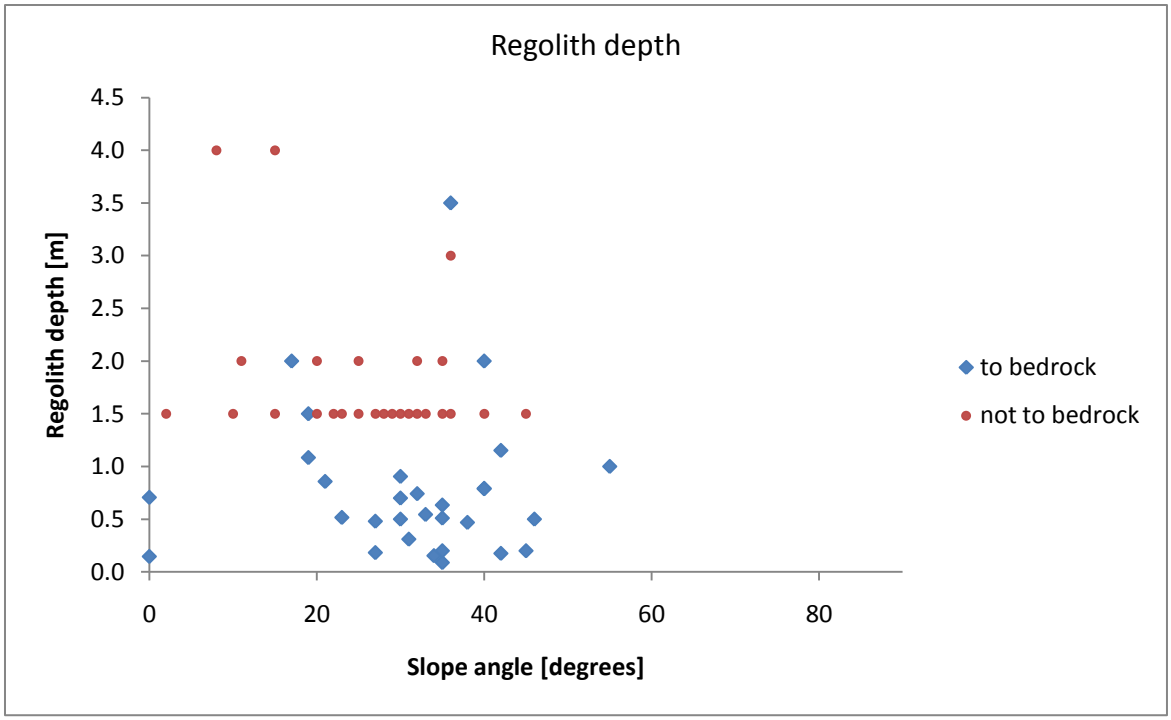

Figure 3. Regolith depth and slope angle. Red dots indicate regolith depths larger than the maximum measurable depth.

3.1.3 SHEAR STRENGTH

Results of the dry shear strength tests for the three tested samples are displayed in Figure 4. Because differences between the three samples are small and there are no systematic deviations, one trend line is based on the points of all samples. The dry shear strength results have been converted to simulated saturated shear strength. The change in strength from dry to simulated saturated conditions can be seen in Figure 5.

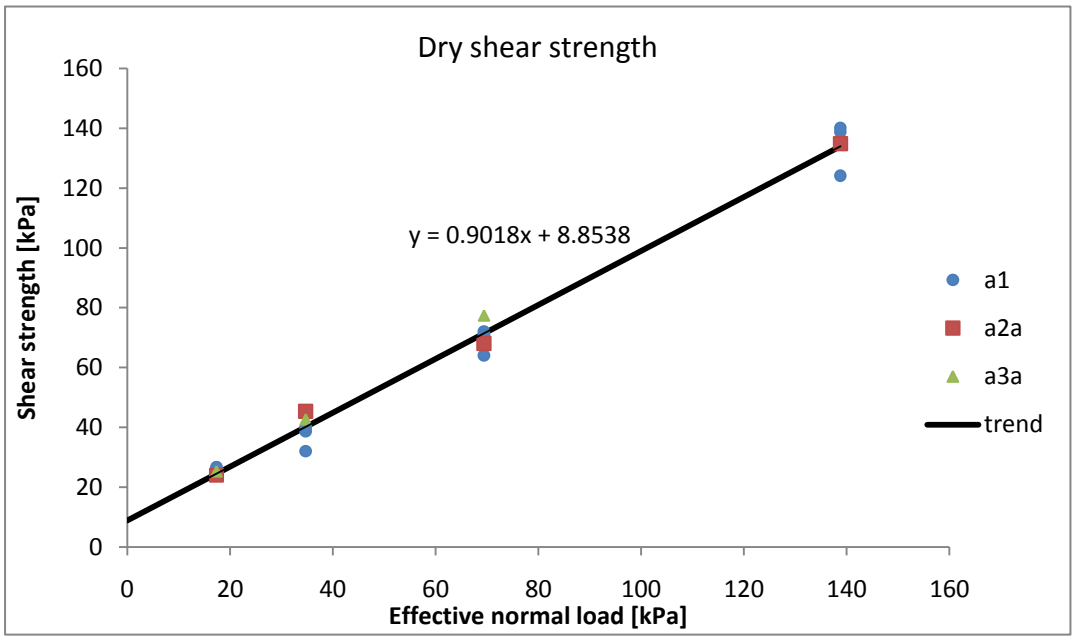

Figure 4. Dry shear strength measurement for three different samples

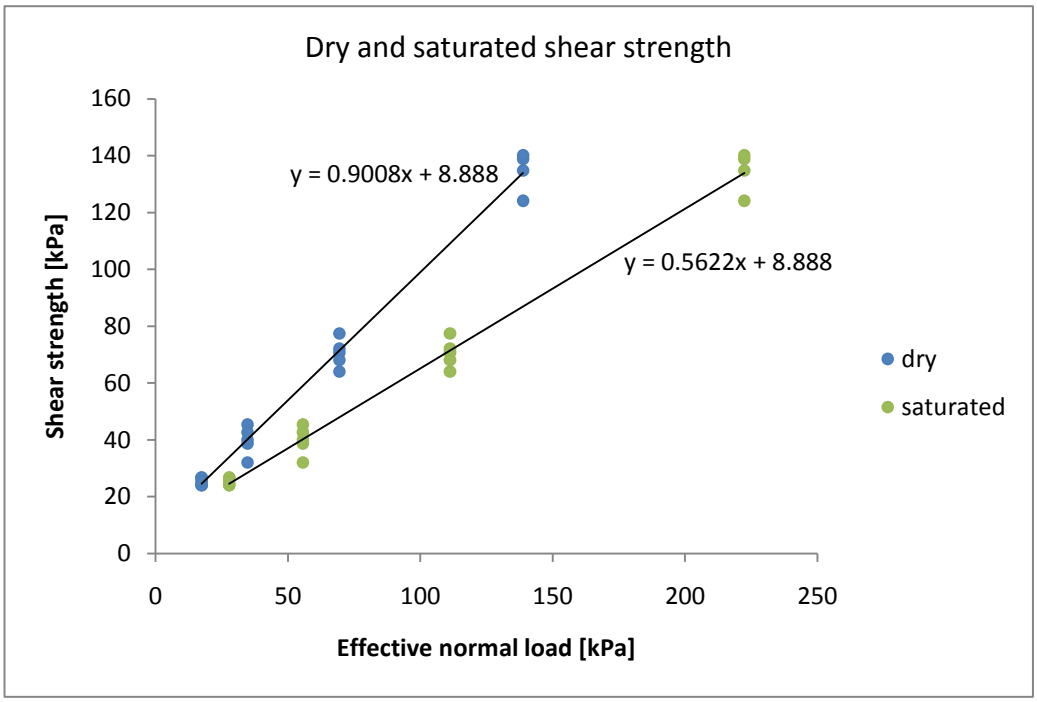

Figure 5. Dry and simulated saturated shear strength

The soil cohesion and angle of internal friction for both dry and saturated conditions are calculated from the regression lines. The resulting input values for the model are shown in Table 2. The soil cohesion values estimated with this procedure are approximately 20 times lower than in situ hand measurement (Torvane) results in Braakhekke (2007). The accuracy and applicability of the in situ hand measurements in the catchment are however doubted, after own measurement yielded unrealistic values. The range of 0 – 10 kPa is in the range of common literature values for forested mountainous catchments (e.g. Selby, 1993; Irfan and Tang, 1992; Bathurst et al., 2009).

Table 2. Soil cohesion and angle of internal friction

	Soil cohesion c_s[kPa]	Angle of internal friction φ [°]
dry	8.9	42.0
saturated	8.9	29.4

3.1.4 INITIAL VALUES

The initial values and their sources are listed in Table 3. These values will form the model input for step 1. For validation, only the maximum rainfall is adapted to the highest value occurring in the maximum 24 hour intensity rainfall map of the validation catchment, which is 750 mm.

Table 3. Initial parameter values for the calibration catchment.

Parameter	value	unit	Source
regolith depth	1	m	fieldwork
wet soil bulk density	1660	kg m^{-3}	fieldwork
combined cohesion	0.73	-	fieldwork
angle of internal friction	29.4	°	fieldwork
saturated transmissivity	75	$m^2 d^{-1}$	literature
minimum slope angle for maintaining flow	27.0	°	fieldwork
run out length	0.4	-	literature
maximum rainfall	0.960	m	rain station data

With the initial values listed in Table 3, the range of slope gradients being conditionally stable is 59° to 68°. Ideally, this would correspond to the maximum slope angles in the mapped landslide polygons, so all polygons can be predicted from one or a few cells in a narrow range of slope gradients in which landslides initiate. In the calculation of critical rainfall and stability, the model uses the slope of the steepest descent as value for local slope angle θ. From the distribution of the steepest descent (calculated in the model) inside the mapped landslide polygons (Figure 6) can be derived that 80% of the mapped polygons has a steepest slope below 59°. Still, these polygons can be predicted by an unstable cell higher upslope, triggering a landslide with a path crossing the polygon.

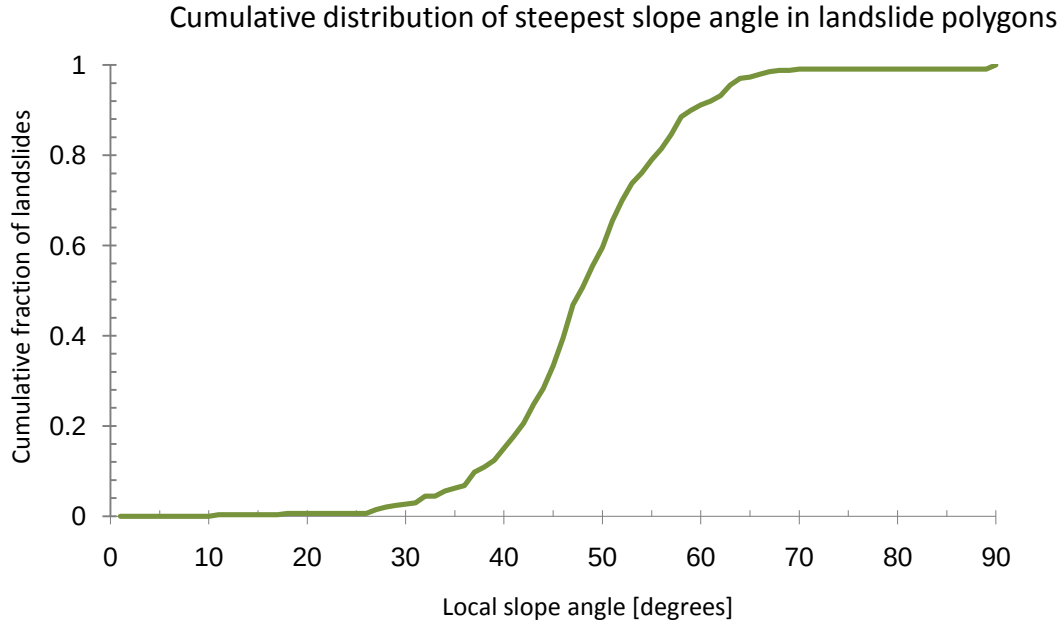

Figure 6. Cumulative distribution of steepest slope in landslides

3.2 SENSITIVITY ANALYSIS

The sensitivity of the model results for changes in the different model parameters has been investigated. For each parameter separately the input has been varied from 50% to 150% of the original input value, with steps of 10%. Because this research is focused on the location of

predicted landslide cells, the influence of parameter change on the total number of cells with predicted erosion is used. Results are shown in Figure 7.

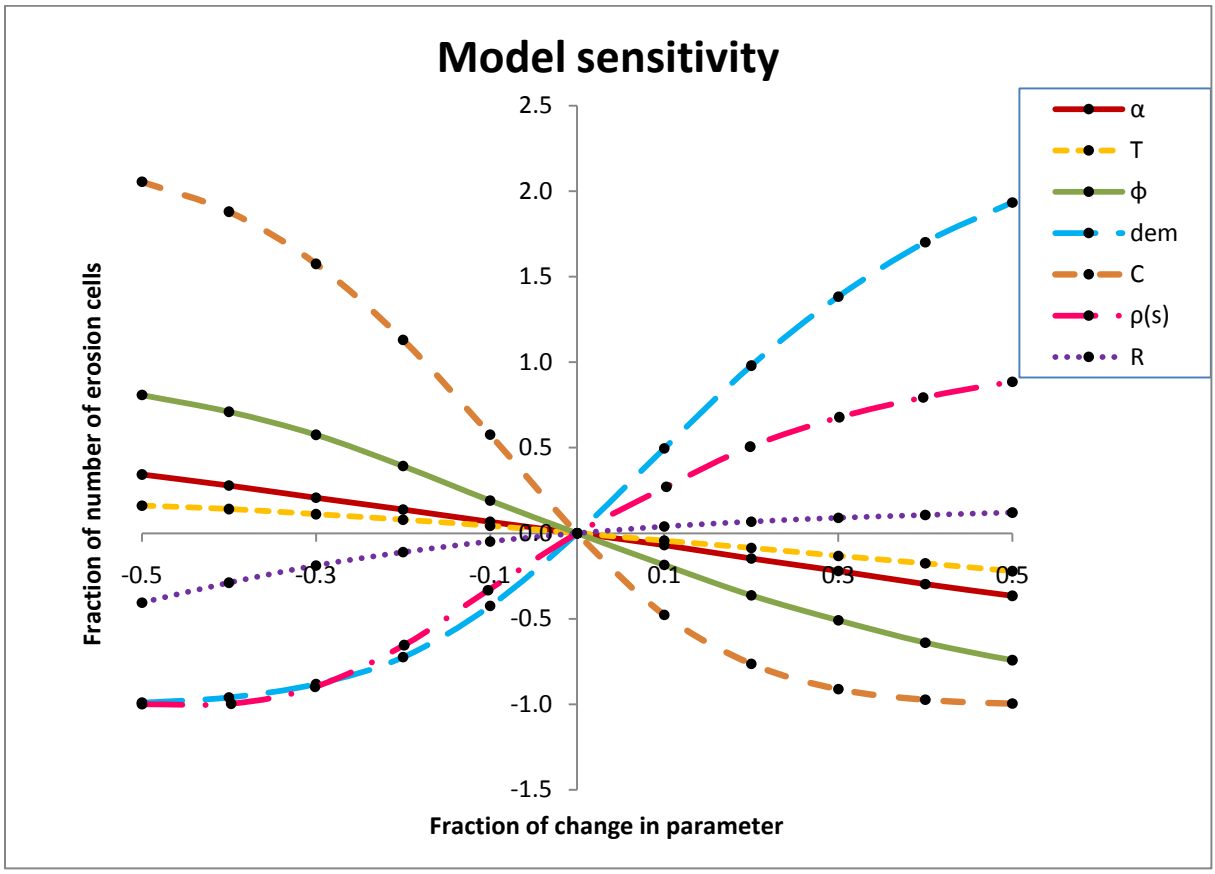

Figure 7. Model sensitivity for selected parameters.

3.2.1 DEM

The digital elevation model influences the model outcome by its resolution. Claessens et al. (2005) showed that a coarser resolution leads to smoothing of the landscape and consequently a lower amount of conditionally unstable cells, as local high gradients are filtered out. To investigate the influence of slope angle, the DEM elevation has been changed from -50% to +50%. The results show a strong increase with increased vertical exaggeration. This can be explained by the dependence of the critical rainfall of slope angle and by the increased length of the erosion path.

3.2.2 COMBINED COHESION (C)

Combined cohesion is the ratio between forces resisting failure and forces promoting failure. Because *C* is used for calibration, its constituents C_s, C_r, and *h* are not treated separately in this sensitivity analysis.

The combined cohesion partially determines the stability and critical rainfall calculations (equation 5, 6 and 7). The number of cells classified as unconditionally stable increases with increasing combined cohesion, the number of cells classified as unconditionally unstable (representing bare rock) decreases (Figure 8). This can be explained by a relatively higher share of failure resisting forces. With initial values, 98% of the cells in the catchment are classified as

stable and approximately 0% is unstable, leaving 2% of cells available for landslide initiation. The number of cells that are available for landsliding is strongly dependent on combined cohesion and the model outcome is thus highly sensitive to changes in combined cohesion.

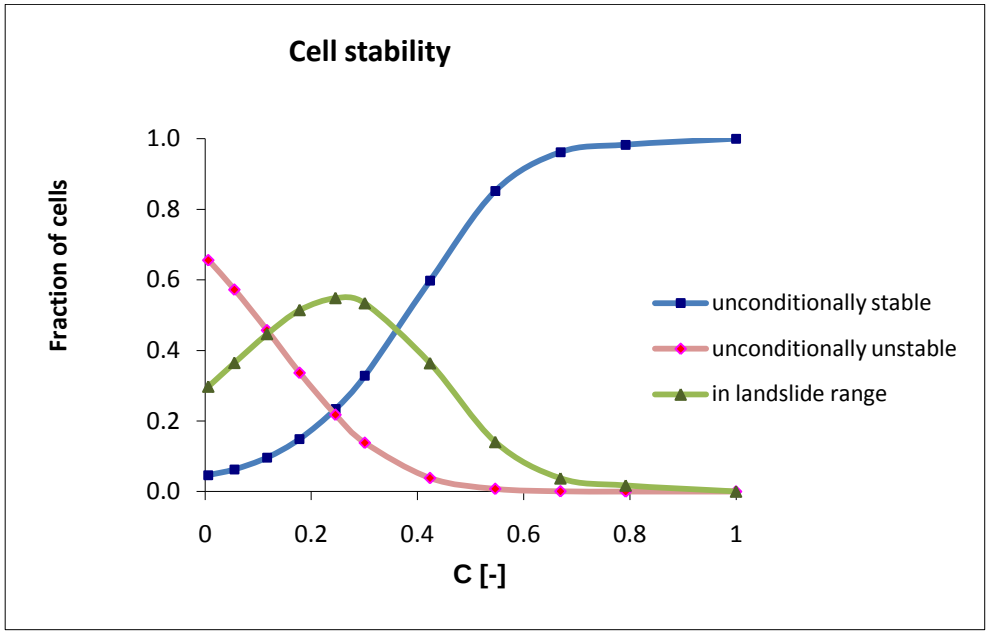

Figure 8. Distribution of cell stability at different values of C.

3.2.3 PRECIPITATION (R)

The amount of rainfall that is applied in the model is not part of any equation, but determines the critical rainfall value below which cells will become unstable. If the critical rainfall Q_{cr} of a cell is higher than the applied precipitation R, the cell requires more rainfall to become unstable and will not initiate a landslide. The sensitivity in Figure 7 seems low, but because the initial value for R is already very high, the number of cells that are additionally triggered at higher R is low. In fact, the amount of precipitation is a strong determinant of the number of cells with predicted erosion. At lower values, both are linearly related.

3.2.4 ANGLE OF INTERNAL FRICTION (φ)

The angle of internal friction is part of the critical rainfall calculation and the calculations for unconditional stability and instability (equations 5, 6 and 7). Physically, a higher angle of internal friction means a higher resistance against shear stress. An increase of 1° moves up the calculated boundaries for unconditionally stable and unconditionally unstable cells with approximately 1° and increases the critical rainfall with 30 mm, which corresponds to the physical meaning of internal friction. Because the amount of cells per slope class decreases after 40°, the shifting up of boundaries of stability decreases the number of cells that are only conditionally stable. The combined effect of shifting boundaries and higher critical rainfall lowers the number of cells with predicted erosion.

3.2.5 SATURATED BULK DENSITY (ρ_s)

The value for saturated bulk density (ρ_s) is present in combined cohesion C (equation 3) and in the calculation of the slope limit for unconditional stability (equation 6). A higher ρ_s yields a

lower *C*, because the weight of the regolith is higher, which increases the forces enhancing failure. Furthermore, the slope limit for unconditional stability becomes lower.

The influence of ρ_s on critical rainfall is more complex, because both ρ_s per se and *C* are present in the equation. For the term containing ρ_s, a higher bulk density leads to higher critical rainfall. This can be explained as the weight of water relative to soil is less, requiring more water for an equal relative increase in weight. For the term containing *C*, a higher bulk density leads to a lower *C* and consequently a lower critical rainfall. This is because a higher weight increases the forces promoting failure. Which of the two terms is dominant is dependent on the slope angle (θ) and the other factors determining *C*. At slope angles that are larger than a certain value, a higher ρ_s leads to lower critical rainfall. At more gentle slopes, higher bulk density leads to higher critical rainfall. This is illustrated for 7 different slope angles in Figure 9. The threshold value for increasing or decreasing rainfall is dependent on and approximately equal to the angle of internal friction φ.

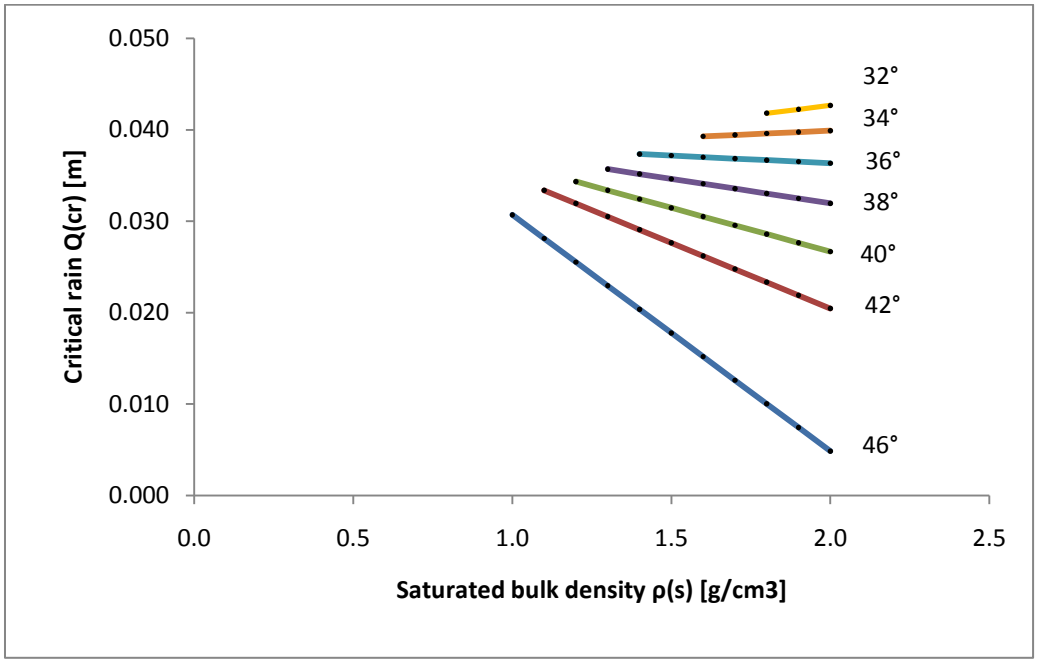

Figure 9. Critical rainfall for indicated slopes angles (c_s = 5 kPa, φ = 35°). Decreasing length of lines is caused by the changing slope limits for unconditionally stability.

At high *C*, the decreasing term is always stronger than the increasing term. The effect illustrated in Figure 9 therefore only occurs at low values for *C*.

Combining the effects of changing slope limits for stability, influence on *C* and the critical rainfall, the number of cells with predicted erosion increases for increasing bulk density.

3.2.6 TRANSMISSIVITY (T)

In the critical rainfall calculation, transmissivity *T* is linearly related to the critical rainfall Q_{cr}, and as such has a minor influence on the number of cells with predicted erosion. At higher transmissivity, a cell requires more rainfall to become saturated and induce a landslide, which, at equal amounts of rainfall, decreases the number of cells that reach their critical rainfall and therefore become unstable.

3.2.7 CRITICAL ANGLE (α)

Changing the minimum local slope required for debris flow leads to a weak linear response in amount of predicted erosion cells. An increase in this parameter leads to deposition at higher local slope angles and thereby shortens the erosion path and lowers the amount of cells active in landsliding.

3.3 CALIBRATION AND VALIDATION RESULTS

3.3.1 MODEL PERFORMANCE RESULTS

The model performances for step 1, 2 and 3 are listed in Table 4 for the calibration catchment and in Table 5 for the validation catchment. US values are the slope angle below which cells are classified as unconditionally stable, UU values are the slope angle above which cells are classified as unconditionally unstable, both resulting from the calibrated parameter combinations.

Table 4. Model performance for the calibration catchment.

	msr	landslide prediction	stable cell prediction	C [-]	R/T [m^{-1}]	ϕ [°]	US [°]	UU [°]
step 1	0.565	0.147	0.983	0.73	0.0130	29.4	59	68
step 2	0.772	0.755	0.790	0.27	0.0009	38.9	33	52
step 3 precipitation	0.783	0.769	0.797	0.26	0.0010	35.9	30	48
step 3 land use	0.789	0.787	0.790	see Table 6		35.4		

Table 5. Model performance for the validation catchment.

	msr	landslide prediction	stable cell prediction	C [-]	R/T [m^{-1}]	ϕ [°]	US [°]	UU [°]
step 1	0.547	0.103	0.992	0.73	0.0130	29.4	59	68
step 2	0.724	0.732	0.718	0.27	0.0009	38.9	33	52
step 3 precipitation	0.734	0.712	0.756	0.26	0.0010	35.9	30	48
step 3 land use	0.735	0.750	0.719	see Table 6		35.4		

Step 1

Using the initial parameters values, the amount of landslides that is correctly predicted is low in both cases, whereas the stable area prediction is very high. This indicates an under-estimation of landslide area and can be caused by over-estimation of combined cohesion C or under-estimation of the rainfall parameter R/T. Landslides are initiated on the steepest slopes only and their predicted locations do not compare well with the landslide inventory map.

Step 2

By running the model for the indicated range of C, R/T, and φ in step 2, the performance is optimised both for calibration and validation without adding extra information. The MSR increases due to an improvement in landslide prediction, but this has come at the cost of correct prediction of stable cells. The optimal combination consists of lower C, lower R/T and higher φ. The range of slope angles within which landslide initiation can take place has shifted down to the range of the lower 50% of landslides in Figure 6. Landslide polygons with a steepest slope

higher than 52° can still be predicted, but the landslide initiation point in the model is not their steepest cell.

Another important observation is that the combined cohesion value for the 10 best model performance runs are all in the range of 0.2 to 0.3, at which the number of cells that are available for landsliding is the largest (Figure 8), or the least of cells are excluded from landslide initiation. This leaves the model the most possibilities to initiate landslides, which is important in order to predict a high number of landslides.

For the entire range of C, R/T, and φ values, the resulting model performance in the calibration runs has been plotted in Figure 10. It clearly shows the trade-off between a good performance in predicting landslides and a good performance in predicting stable areas. For the point with the best performance, a change in parameter values always results in an improvement in either landslide or stable cells prediction that is smaller than the decrease in performance for the other, resulting in a degraded all round performance. Another observation than can be made is that although a 100% performance can be achieved for stable cell prediction, this cannot be achieved for landslide prediction. There is a group of landslide polygons (approximately 20% of the total number) that is not easily predicted, and their prediction comes at the cost of 50% in stable cell prediction. This inability is probably an effect of the DEM resolution and is further discussed in section 3.5.

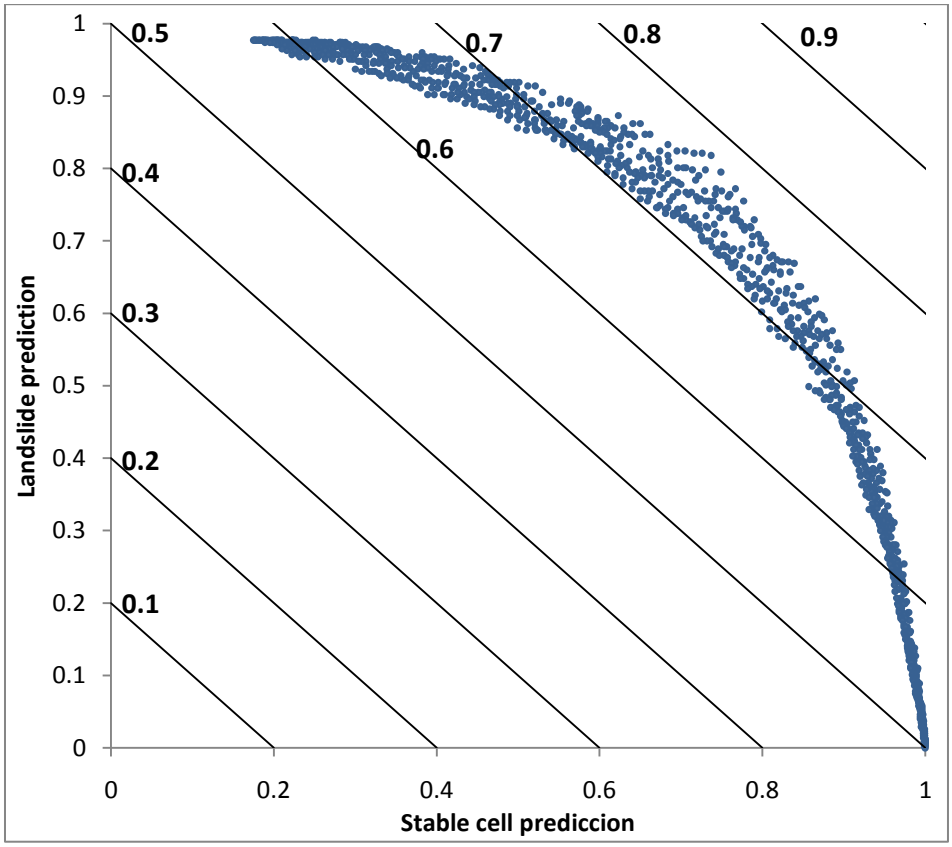

Figure 10. Model performance for calibration step 2, MSR indicated as diagonals.

Step 3 – spatial distribution of rainfall

The model performance improves by adding the spatial distribution of rainfall. The increase in MSR is caused by a better performance in predicting stable cells, whereas the number of

correctly predicted landslides has decreased. Although the rainfall map derived from radar provides a good estimate of maximum 24 hour rainfall, local extremities are still not known because of the coarse resolution (1 km grid). The forest canopy can however smoothen the precipitation intensity (Keim and Skaugset, 2003), reducing this effect of local variability. Other rainfall factors might be equally important in determining landslide locations, for instance rainfall duration (Chiang and Chang, 2009; Frattini et al., 2009), antecedent rainfall conditions (Crozier, M.J., 1999; Ibsen and Casagli, 2004; Frattini et al., 2009), or temporal rainfall pattern (Tsai, 2008) especially when predicting on a short time scale. These factors are however not included in the LAPSUS-LS model and more detailed model equations are necessary to incorporate these effects (e.g. non-steady state hydrology or modelling a single event in multiple time steps), leading to higher data requirements.

Step 3 – land use stratification

Because in previous steps the number 10 runs with best performance had very different values for φ and φ is expected to be dependent on regolith composition only, a constant value for φ for all land use types is chosen to reduce the amount of necessary optimisation runs. The average of the 10 best runs of step 2, 35.4° is considered representative. The calibrated parameters for the different land use types are displayed in Table 6.

The implementation of land use stratification leads to an increase in performance. The MSR increase for this run is the result of better actual landslide prediction, as opposed to the improvement added by the rainfall map. The model is most sensitive to changes in broad-leaf and needle-leaf parameters, as these cover 95% of the catchment area. Parameters for agricultural areas do not influence model performance, as these are only on near-flat areas where no landslides occur.

Table 6. Calibrated parameter values per land use type.

	broad-leaf forest	needle-leaf forest	arrow bamboo	agriculture	bamboo patches
C [kPa]	0.26	0.26	0.13	0.40	0.18
R/T [m^{-1}]	0.0008	0.0008	0.0010	0.0010	0.0010

The combined cohesion of the broad- and needle-leaf forest is similar and higher than the calibrated combined cohesion of both bamboo types. Higher combined cohesion can be associated with higher root or soil cohesion, lower soil depth or lower bulk density. Because the fieldwork measurements of soil cohesion, regolith depth and bulk density did not show clear difference among land use types, the most likely cause is difference in root cohesion. The calibrated values correspond to the observations of the shallow rooting of bamboo vegetation, not deeper than the estimated 1 m depth of the shear plane. Parameter variation within a land use type can be high (e.g. Greenway, 1987; Schmidt et al., 2001), but is not accounted for in this research.

Small differences in rainfall parameter *R/T* for the different land use types could represent vegetation effects on the amount of precipitation that actually reaches the surface (*R*) through canopy storage and interception (Greenway, 1987; Van Beek and Van Asch, 2004; Keim and Skaugset, 2003) or differences is transmissivity *T*, possibly by rooting. The higher *R/T* value found for arrow bamboo and bamboo patches would physically represent a higher amount of

required applied rainfall *R*, meaning a lower fraction of the total rainfall that actually contributes to landsliding, or a lower transmissivity *T*, likely to be caused by the less shallow rooting.

3.3.2 DIFFERENCE BETWEEN CALIBRATION AND VALIDATION PERFORMANCE

For all runs, validation model performance is lower than the performance for the calibration catchment. A possible cause could be the difference in data sources for the landslide inventory maps. The landslide inventory map for the calibration catchment is compiled specifically for the Aere event, whereas the map used for the validation catchment is made for 2005. Furthermore, data of the calibration DEM are floating point, while the validation DEM data type is integer. The possible effects of these differences in data are not clear, but they could cause a certain discrepancy.

Other possible causes for the lower performance could lie in the different physical parameters of the two catchments. Half of the validation area consists of a meta-sandstone, which does not occur in the calibration catchment. Excluding this sandstone area from the validation however does not yield better results. The higher average slope in the validation catchment (Figure 2) would lead to a higher landslide density, but the opposite is true. This can be explained by the lower amount of rainfall for the validation area in the Aere typhoon event. Although the lower amount of rainfall is accounted for in the modelling, the model calibration does not appear optimal for the validation catchment. This might indicate that the model's linear response to lower rainfall conditions is not similar to the response in reality. The different rainfall conditions in the validation catchment might therefore require a different parameter combination for optimal performance.

When applying the land use calibration methodology (step 3) to the validation catchment, optimal *C* values area approximately 15% lower and *R/T* (after applying the lower maximum rainfall for the validation catchment) approximately 20% for the largest land use types. The optimal model performance is however still lower than for the calibration area. Strictly physical, this might indicate a higher average regolith depth in the validation catchment: an increase in regolith depth *h* causes a lower *C* (equation 3) and, although not implemented in this model, a higher transmissivity *T* if calculated as product of horizontal conductivity and regolith depth. This could result from a systematically lower rainfall, leading to lower landsliding and erosion rates and therefore thicker regolith. On the other hand, the lower landslide density could also suggest a decrease in landslide potential, caused by more frequent landsliding in the recent past, thereby decreasing average regolith depth. A systematic landslide inventory for recent years could test these hypotheses.

Disregarding the physical meaning, the lower *C* and *R/T* values might as well represent a model set up aimed at lower rainfall conditions and lower landslide density, without any physically meaningful explanation of the change in values.

3.4 APPLICATION RESULTS

Model results of the land use change scenario are displayed in Figure 11. Landslides predicted in the original state remain in place, and new landslides are triggered at positions that have undergone a change in land use and start to cover the original agricultural fields, showing the

off-site effects of upslope changes. The emergence of new landslides is caused by decreased stability because of a decline in root cohesion. Most new landslides are relatively small, as the slope angle at which these new landslide occur are close to the minimum angle for maintaining flow (27°) because of the low C in equation 6. This particular increase in small sized landslides after logging is also reported in Guthrie (2002) and Imaizumi et al. (2008), based on actual landslide inventory maps.

The scenario is simple and not realistic in all ways. Clearing of forests is not likely to happen in all directions, but will rather focus on suitable places for agriculture or construction. Furthermore, root cohesion does not decline instantaneously after forest clearing, but has a gradual decline (Sakals and Sidle, 2004). However, the main purpose of the applications is to show an example of the capability of the model to simulate the possible influences of land use change on shallow landslide susceptibility.

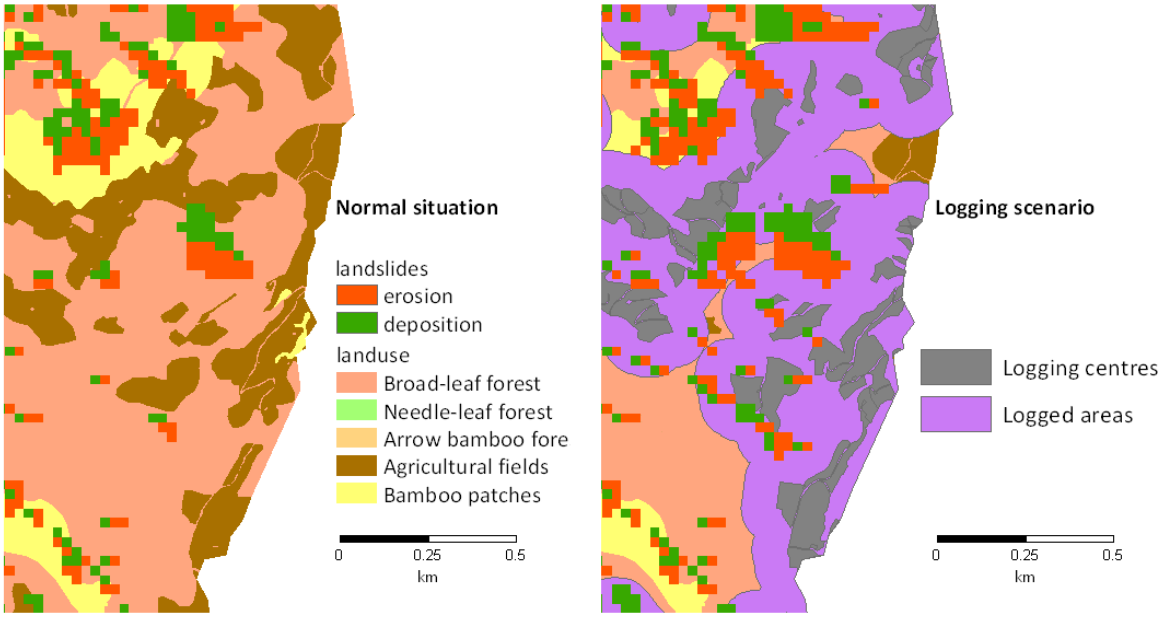

Figure 11. Part of the calibration catchment, showing additional landslides triggered in the area of forest clearance.

3.5 INFLUENCE OF MODELLING RESOLUTION

Several researchers have studied the effect of modelling resolution on landscape modelling (e.g. Schoorl et al., 2000; Gertner et al., 2002; Claessens et al., 2005). In general, the modelling resolution has a significant influence on the model outcomes. At coarser resolutions, the contributing areas (a) become larger and the local slopes (θ) decrease (Wilson et al., 2000, in Claessens et al., 2005), which influences the calculation of for example the critical rainfall Q_{cr} (equation 5). The influence of modelling resolution on LAPSUS-LS output has been studied in detail by Claessens et al. (2005). However, the influence of DEM resolution on the actual model performance in landslide location prediction is less well known. The model performances at the range of parameter values used for calibration step 2 are displayed in Figure 12 for a DEM resolution of 9 m, 27 m, 54 m and 81 m.

It is clear that model performance increases at finer resolutions. The maximum amount of actual landslide polygons that can be predicted is 100% at 9 m, 98% at 27 m, 82% at 54 m and 67% at 81 m. Both the ability to predict a landslide and ability to predict a stable area increase, showing that the model is better able to discriminate between unstable and stable. This is in agreement with findings of Lee et al. (2004) for a statistical model and Tarolli and Tarboton (2006) for a similar infinite slope and steady state hydrology model. Dietrich and Montgomery (1998) also found that at finer resolutions, instabilities can be mapped more precisely. Tian et al. (2008) reported a second performance optimum at coarse resolution, but this is not found in other studies.

The dependence of model performance on the modelling resolution can be explained as an effect of smoothing: at coarse resolutions, certain fine local topographic triggers, i.e. steep areas, are lost. The mean and standard deviation of slope angle decrease (Table 7), meaning less potential for landslides and loss of local topography that can be the initiation point of landslides. This results in elimination of possibilities to discriminate between landslide and stable area and this is reflected in the curves of Figure 12: an equal increase in landslide prediction comes at a higher cost of stable prediction.

Besides the better representation of local slope angles, also the hydrological patterns and debris flow routing are likely to be in better correspondence with nature at fine resolution (Garbrecht and Martz, 1994), reducing the inaccuracies in the stream network and debris flow routing. Tarolli and Tarboton (2006) find that performance decreases again at resolutions finer than 10 m, and suggest that this is because at finer resolutions, the local surface topography is likely to be less representative of the underlying bedrock topography. As the bedrock topography can dominate the subsurface flow (Freer et al., 2002), the bedrock topography essentially influences landslide initiation. In that case, fine scale topography is less representative for the processes governing the landslide initiation.

Table 7. Slope statistics at different DEM resolutions.

DEM resolution [m]	average slope angle [°]	standard deviation [°]
9	34.2	12.6
27	32.7	10.1
54	30.1	9.0
81	27.9	8.5

At finer resolution, the combined cohesion C for the best run is higher (0.4 at 9 m, against 0.2 at the other resolutions), meaning that the required stability is higher. The slope range in which landslides can initiate is higher (39° - 55°) and these values are closer to the values found in the field (Figure 6 and

Table 3), which supports the idea that the finer resolution better resembles reality, although care should be taken in comparing lumped modelled values to point measurements.

Even though modelling at 9 m resolution performs better in this case, the 27 m results still demonstrate the model's ability to perform satisfactory results at coarse resolution and the relative differences between the modelling steps and land use types are found to be valid across different resolutions.

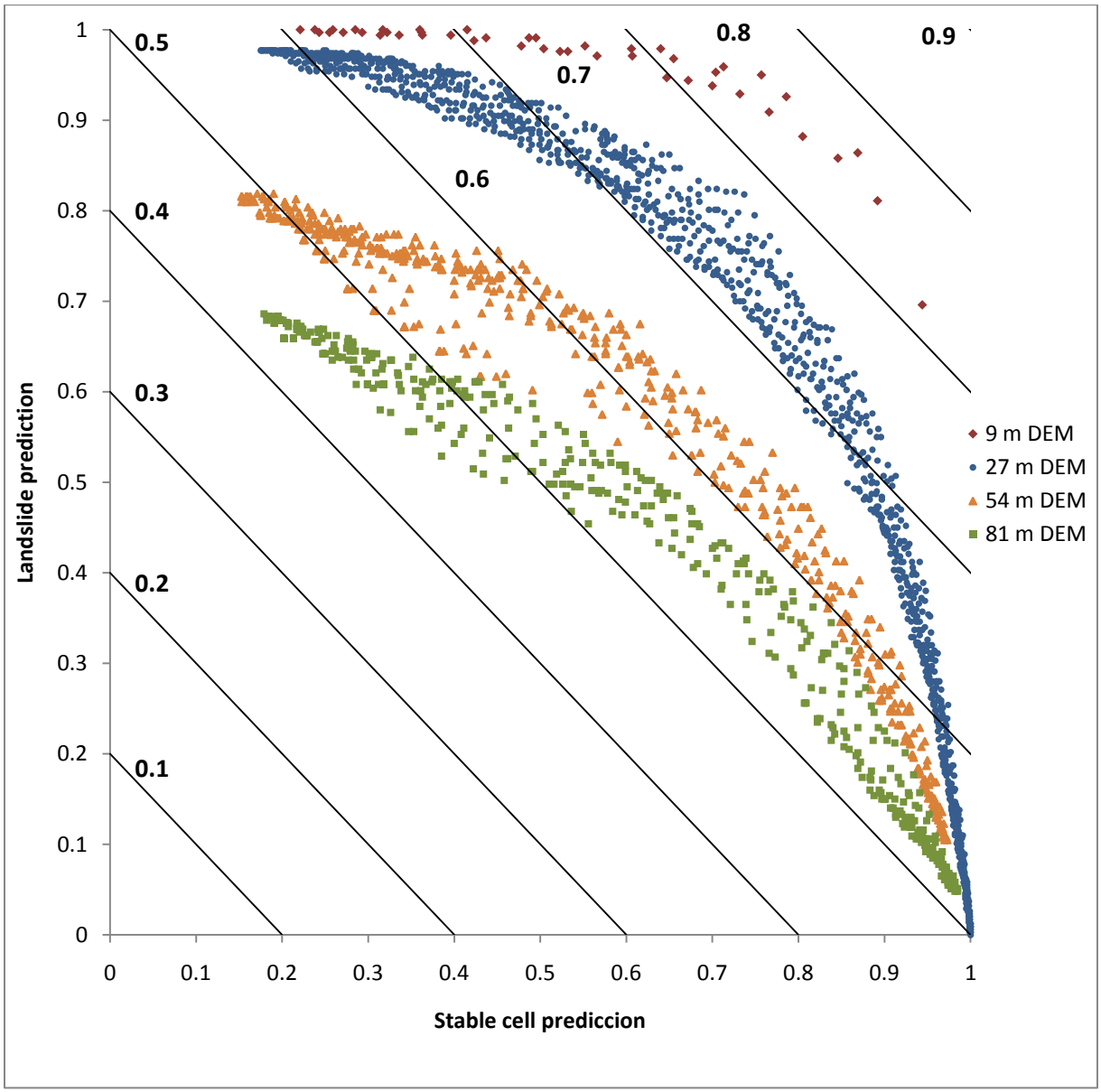

Figure 12. Model performance for calibration step 2 at different modelling resolutions. Less model runs are done for 9 m resolution because of the long computation time.

3.6 GENERAL MODEL PERFORMANCE

For the calibration and validation runs with the 27 m DEM as demonstrated in section 3.3.1, on average 75% of the landslide polygons is correctly predicted. These correctly predicted landslides are mainly the polygons that directly border streams and have an area of multiple cell sizes (Figure 13). The polygons that are not predicted are often located on gentler slopes and are relatively small. This is likely to be caused by the relatively coarse resolution of the model, as the results in section 3.5 indicate: small irregularities in topography are lost at coarse resolutions, losing possible initiation points and increasing uncertainty in the routing of the landslide downslope. Furthermore, possible landslide initiation points induced by humans, e.g. road constructions, are not incorporated in the model.

Another cause for the incapability to predict certain landslides can be the assumption of steady state hydrology. This assumes that subsurface flow follows topographic gradients and discharge and recharge are in equilibrium (Pack et al., 1998). In high intensity rain events however, these assumptions might not be valid (Iverson, 2000; Crosta and Frattini, 2003; Chiang and Chang, 2009). As reported Chiang and Chang (2009), the steady state assumption leads to failure in model prediction of landslides with a small contributing area or a gentle slope. For this study, the average contributing area for cells in landslide polygons that were not predicted, is however not significantly smaller than the average in predicted polygons.

For both calibration and validation, the amount of landslides in calibrated runs is over-estimated, hence the lower score in stable cell prediction. The over-estimation of landslide susceptibility is common in most physically based models, e.g. Borga et al. (1998), Van Beek and Van Asch (2004) and Kuriakose et al. (2009), and is this case is also a result of the way in which the model performance is calculated: at initial parameter values, there is under-estimation of landslide area, but to improve on landslide prediction, a certain over-estimation has to be made.

Some of the incorrectly predicted landslides are located at landslides mapped in the 1976, 1986 and 1992 inventory. This might indicate that the landslide potential has decreased, e.g. the regolith has already been removed in earlier landslides, or the slope stability has increased, and therefore no new landslide took place in the 2004 event. The possible locations of landslides are thus dependent on the landslide record of previous events. This legacy effect is difficult to implement, but is an important factor when trying to model multiple time steps or events in sequence (Claessens, 2005).

Furthermore, assuming a power-law distribution of landslide area and landslide frequency (Malamud et al., 2004; Stark and Hovius, 2001), a large number of small landslides (e.g. smaller than 1000 m^2) is not mapped in the area. In the study area, small landslides have been observed above which the forest canopy was still intact. When compiling a landslide inventory map from air photos, these small entities are invisible and consequently omitted. Landslides predicted at locations without a mapped landslide can therefore indicate an actual instability that is not mapped or has been removed from the dataset in the data preparation phase because of the small area.

Directly comparing the model performance to other studies is somewhat limited by the different methods used to calculate the performance. In most cases, a map of Factor of Safety values

(equations 1 and 2) is compared with a point or polygon dataset of landslides (e.g. Huang and Kao, 2006; Chiang and Chang, 2009). In this research, actual landslide polygons are compared to predicted landslide paths, which adds an extra source of uncertainty or possible error, i.e. the routing of debris flows. Combining a calculated critical rainfall map and a statistical model, Chang and Chiang (2009) achieve a MSR of 0.840 for the same calibration catchment and the same typhoon event with a 10 m DEM. The model performance for a study by Braakhekke (2007), using the LAPSUS-LS model for the same catchment was calculated from critical rainfall values only and success rate for prediction of stable cells was 52.8% and 75.5% for unstable cells (landslide cells). Huang and Kao (2006) used a similar model and comparable methodology for a mountainous catchment in central Taiwan and achieved a maximum MSR of 0.75 at 40 m DEM resolution. Considering differences in modelling resolution and model performance calculation, the LAPSUS-LS model performs well in landslide location prediction.

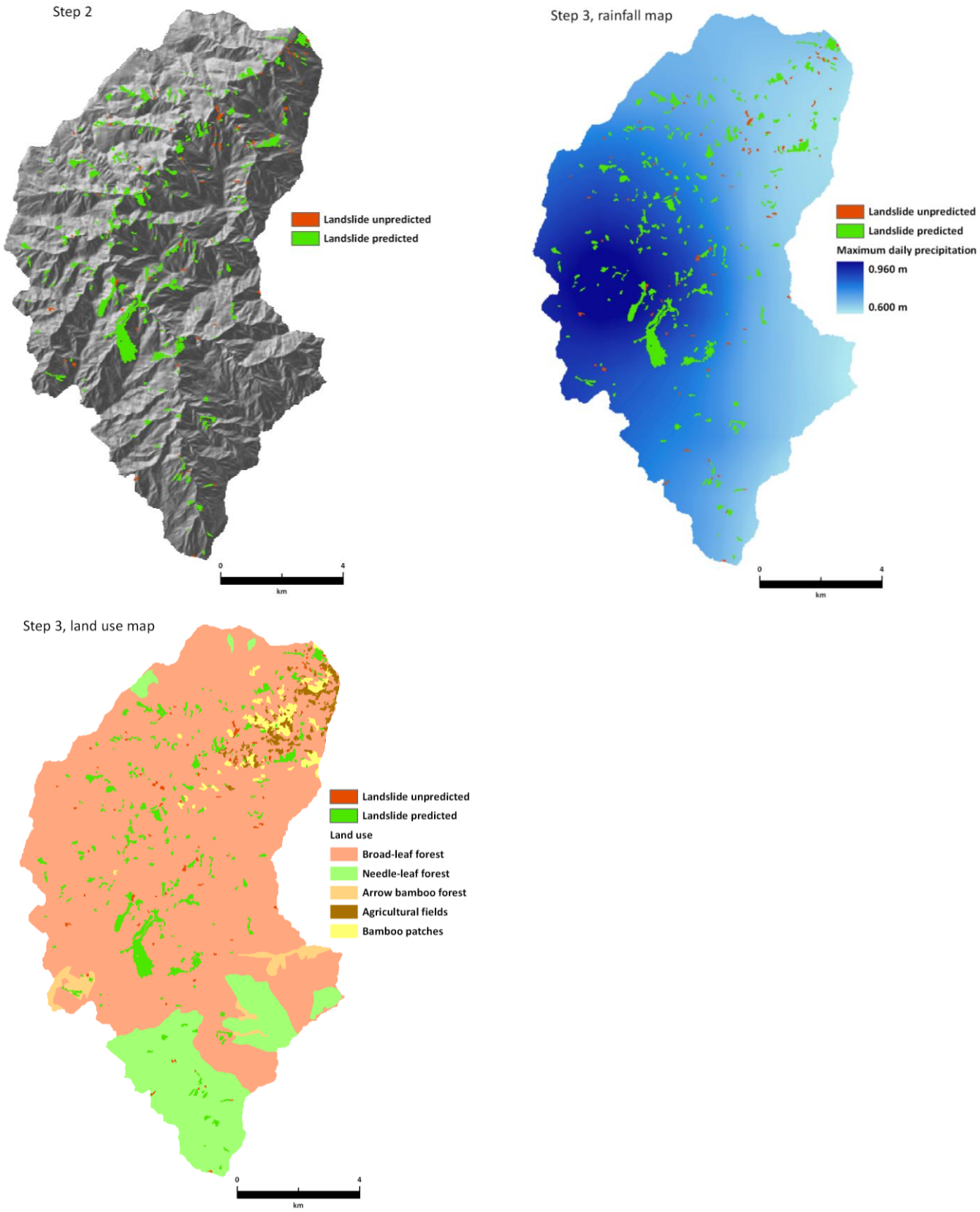

Figure 13. Correctly predicted and unpredicted landslides for step 2, step 3 with rainfall map and step 3 with land use map.

3.7 PARAMETER CORRELATION

Calibration was done by adapting three parameters: *C*, *R/T* and φ. A change in one of these not only influences the model outcome, but also influences the optimal value of the other two parameters. The influence the parameters have on each other is investigated by plotting a contour plot for model performance MSR against two parameters, while the third parameter is kept constant. The plots are displayed in Figure 14.

Both combined cohesion *C* and angle of internal friction φ increase slope stability at higher values, while rainfall intensity *R/T* decreases stability. This is apparent in Figure 14, showing positive relations for *R/T* - *C* (plots 14*a*-*b*) and *R/T* – φ (plots 14*c*-*d*). A negative relationship exists between *C* and φ (plots 14*e*-*f*). In that case, it can be seen that an increase in one has to be compensated by a decrease in the other, as both parameters enhance slope stability in the model. In this case, 10° of internal friction is approximately equal to 0.05 of *C*. When the applied rainfall increases, either *C* or φ has to be higher to have an optimal performance: the higher forcing has to be compensated by a higher resistance.

In all plots, there is a clear range of optimal combinations that have a similar model performance, although the position of these ranges can change rapidly when the value of the constant parameter is changed. The ranges of optimal combinations represent different parameter combinations that have similar model performances. This equifinality often occurs in physical modelling (Beven and Freer, 2001) and without further field measurements, one cannot select the most realistic of combinations (Huang and Kao, 2006). Deviations from the optimal combinations, i.e. decrease or increase in one of the parameter values, lead to lower model performance. These optimal ranges represent the nature of the equations on which the model is based and do not necessarily point to realistic combinations of parameter values. Still, these images can guide the calibration process by showing the range of values to focus and give insight in the correlation that parameters have in the model.

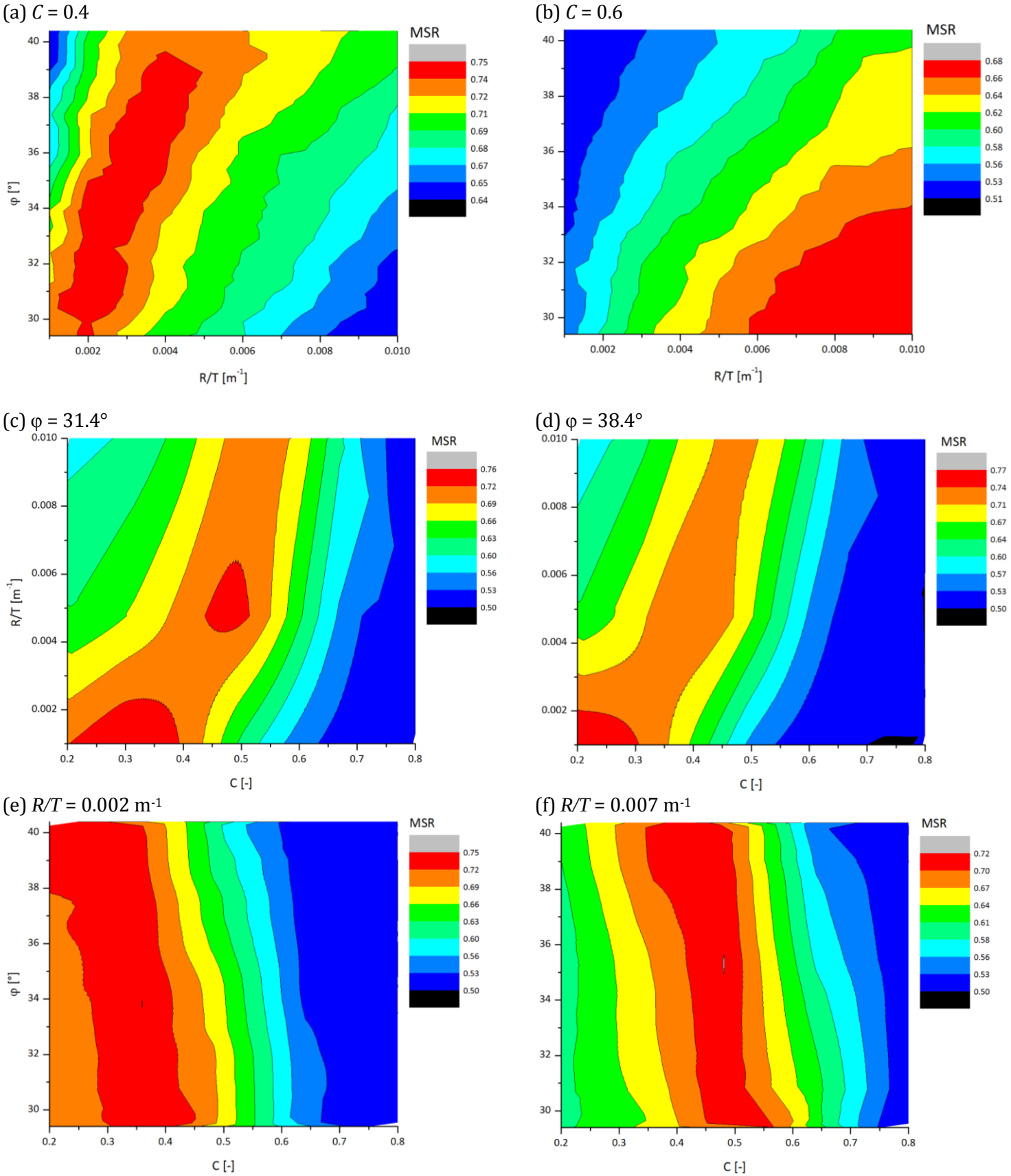

Figure 14. Model performance contour plots for constant *C* (a and b), constant φ (c and d) and constant *R/T* (e and f).

3.8 INITIAL PARAMETER VALUES AND CALIBRATED VALUES

The parameter values that turned out to be optimal for landslide prediction in this study deviate from the initial input values. Some changes are expected, others are not. The difference between measured values and the optimal model calibration is discussed in this section.

First, combined cohesion *C* in all calibration runs is over 50% lower than the value calculated from fieldwork. The calibrated lower value, in reality, would represent a lower soil or root cohesion or higher bulk density or regolith depth. In the model, the main reason for lowering of combined cohesion is to change the range of slope angles that are available for landslide initiation. To allow this lowering and not run into dramatic over-prediction of landslides, *R/T* has decreased ten-fold.

In the case of the angle of internal friction (φ), a higher value was found in calibration. This was expected, as in the laboratory analysis only the fraction of regolith smaller than 2 mm was used for determination of soil cohesion and internal friction angle. At increasing content of coarse fractions, the shear strength will increase (Rahardjo et al., 2008) and mainly because the angle of internal friction increases, following equation 11 (Irfan and Tang, 1992). As found in the bulk density laboratory analysis, on average 36% percent of the sampled regolith volume consists of particles larger than 2 mm. Using the relation between coarse fraction content and internal friction angle established by Irfan and Tang (1992), this would correspond to an increase of 5 to 10° in the angle of internal friction, which is indeed found after calibration. However, as shown in Figure 14*a*, *b*, *e* and *f*, the optimal value of φ also depends on the other calibrated values.

In general, the difference between the measured values and calibrated optimum values for *C* and *R/T* can be attributed to scaling effects and model abstractions. Field measurements are done at a single point or cm scale in the landscape and are assumed to represent a 27 m grid cell or even an entire catchment. However, processes important at the point scale do not necessarily act with the same intensity at grid cell scale and vice versa, which falsifies that assumption. Especially in hydrological processes, non-linearity makes it impossible for a point measurement, both in time and space, to represent a spatial average on a longer time scale (Beven, 1989). A spatial average then again neglects the important spatial heterogeneity that is associated with nearly all parameters (e.g. Borga et al., 1998; Burton et al., 1998). Therefore, by lumping parameter values to grid cells, uncertainty and abstraction of reality are inherently introduced.

In the calibration process of this study, the initial physically meaningful parameters of a physically-based model lose (some of) their physical meaning. Relative differences rather than exact values should be used for conclusions. Although the model performance is optimal at a certain parameter combination, it does not mean that the optimal values are the best representations of reality, but rather the optimal combination of parameter values given the model abstractions, the way of calculating model performance calculation and the modelling resolution. The physical meaning is in this case compromised by a better performance.

4 CONCLUSIONS

LAPSUS-LS, a simple physically-based model can be used to study the landslide – landscape system and investigate the possible effects of parameter changes, for which it is originally designed. The model does not require many inputs and the required values are relatively easy to measure, or readily available in literature. To extend the model's use to prediction of reality, calibration is necessary and this can significantly improve the performance. But, after calibration, the initially measurable physically meaningful parameters lose their physical meaning and become model parameters, relating more to the model structure, scaling effects and parameter correlation. Then, relative changes in parameters and outcomes are more important than the exact values they have, but the results can still provide useful insights.

In general, the initial parameter values derived from fieldwork and literature are comparable to other literature sources. Sensitivity analysis shows that the model is very sensitive to changes in *C* and moderately sensitive to φ. At lower ranges of rainfall *R/T*, the model is very sensitive to changes in *R/T*.

The initial values turn out to be sub-optimal for model performance calculated with MSR. Calibrating by changing combined cohesion *C*, rainfall rate *R/T* and angle of internal friction φ significantly changes these parameter values. The changes are not necessarily directed towards best representation of nature, but more likely to better combinations for the used set of equations, the way of calculating model performance and the modelling resolution. The low calibrated values for *C* and *R/T* and a relatively minor change in φ move the initial range of slope angles susceptible to landslide initiation from 45° - 58° to 30° - 48° on average. With the lower values, landslides are dominantly triggered at positions with more gentle slopes and a high contributing area. These positions are mainly found downslope, bordering the streams, corresponding to the dominant location of landslides as mapped in this study area.

The spatial distribution of rainfall slightly increases model performance because stable areas are better predicted. As can be seen in the prepared rainfall map, the intensity can differ almost 40% in the calibration catchment. Actual landslide prediction does not increase, but instead has a slight decrease. Actual landslide locations are not strongly related to the maximum rainfall intensity in the event, but are likely to be also dependent on antecedent conditions, rainfall duration and human triggers.

The optimal combination of parameters differs per land use type, broad-leaf and needle-leaf forest having the highest values for combined cohesion and both types of bamboo forest the lowest values. Although the bamboo areas used for calibration are small, the values found seem to correspond with field observations in bamboo forests of landslides at gentle slopes and a very shallow rooting depth, limiting the root cohesion. Differences between land use units in the rainfall parameter *R/T* can represent differences in hydrological responses. Because land use units have dissimilar parameter values, changes in land use type can lead to a change in landslide activity.

After transferring the found parameter combination from the calibration to the validation catchment, model performance in validation is lower than in calibration. The lower landslide density and rainfall experienced in the validation catchment requires adaptation to the parameters for optimal performance. The direction of the adaptation suggests a higher average regolith depth in the validation catchment, possibly as a result of a lower past landslide activity. Another possible cause could be that the model's linear landsliding response to rainfall does not equal reality, where instead non-linear responses might

occur. The different data sources for the DEM and landslide map could introduce another source of discrepancy between calibration and validation.

The amount of landslides that can be predicted is strongly dependent on the modelling resolution. At finer resolutions, the topography better resembles reality and therefore the location of landslides can better be distinguished from stable areas. For the used 27 m DEM, on average 75% of the landslides and 80% of the stable cells are correctly predicted. Compared to other studies, this is a satisfactory result for a medium resolution study.

5 SUGGESTIONS FOR FURTHER RESEARCH

As suggested by many other researchers, a finer DEM resolution can give better results. However, even at very fine resolutions, model abstractions and lack of other data at the same fine resolution limit the representation of reality and hence the model performance. Considering the primary use of the model, i.e. to investigate the influence of parameter changes or scenarios and to get better understanding of the system, other research suggestions are more interesting. The cause of the dissimilarity in landslide density and model performance for the two catchments is not clear. Simple fieldwork campaigns to confirm or falsify possible causes are difficult to set up: it is not possible to measure a difference in average regolith depth without taking unrealistically high amounts of samples. Comparing landslide inventory maps of previous events for both catchments could be meaningful to see if there is a systematic difference in landsliding density.

Another important aspect could be to see whether the LAPSUS-LS model can indeed only model locations of shallow landslides, the purpose it was designed for. In the field several deep seated rotational slides or slumps were encountered and these are also included in the landslide inventory map. The model equations are specifically written for shallow translational landslides, but as most of the mapped landslides can be predicted, the model apparently can also indicate the locations of other types of landslides.

This research focused on the event time scale. To allow the model to run for multiple events or years sequentially, quantitative information is necessary on:

- the production of regolith or total weathering rates;
- the redistribution of soil by other forms of erosion;
- the uplift rate;
- the rate of fluvial incision;
- the recovery time of vegetation on former landslide locations.

These factors all have a certain temporal and spatial scale and include feedbacks on each other, creating a complex system. Integrating these factors in a single model is therefore difficult and requires research, but could prove a useful addition.

A short example of the influence of land use change on landslide susceptibility was shown. The interactions between landslides and land use are however not uni-directional, as landslides also influence land use change or allocation. For areas in which landslides have more interference with human activities, LAPSUS-LS might be a good starting point to combine land use change and landslide models to investigate the influences of land use on landsliding and vice versa.

REFERENCES

Anbalagan, R., Chakraborty, D., Kohli, A., 2008. Landslide hazard zonation (LHZ) mapping on meso-scale for systematic town planning in mountainous terrain. Journal of Scientific and Industrial Research 67 (7): 486-497.

Ardizzone, F., Cardinali, M., Carrara, A., Guzzetti, F., Reichenbach, P., 2002. Impact of mapping errors on the reliability of landslide hazard maps. Natural Hazards and Earth System Sciences 2: 3-14.

ASTM Standard D3080, 2004. Standard test method for direct shear test of soils under consolidated drained conditions. ASTM international.

Bathurst, J.C., Isabella Bovolo, C., Cisneros, F., 2009. Modelling the effect of forest cover on shallow landslides at the river basin scale. Ecological Engineering, in press.

Baum, R.L., Coe, J.A., Godt, J.W., Harp, E.L., Reid, M.E., Savage, W.Z., Schulz, W.H., Brien, D.L., Chleborad, A.F., McKenna, J.P., Michael, J.A., 2005. Regional landslide-hazard assessment for Seattle, Washington, USA. Landslides 2 (4): 266-279.

Beven, K., 1989. Changing ideas in hydrology - The case of physically-based models. Journal of Hydrology 105: 157-172.

Beguería, S., 2006. Validation and evaluation of predictive models in hazard assessment and risk management. Natural Hazards 37: 315-329.

Beven, K., Freer, J., 2001. Equifinality, data assimilation, and uncertainty estimation in mechanistic modelling of complex environmental systems using the GLUE methodology. Journal of Hydrology 249: 11-29.

Borga, M., Dalla Fontana, G., Da Ros, D., Marchi, L., 1998. Shallow landslide hazard assessment using a physically based model and digital elevation data. Environmental Geology 35 (2-3): 81-88.

Braakhekke, M., 2007. Landslides under construction: modeling controls on slope stability in a mountainous watershed, Taiwan. Minor Thesis, Wageningen University, The Netherlands.

Burton, A., Arkell, T.J., Bathurst, J.C., 1998. Field variability of landslide model parameters. Environmental Geology 35 (2–3): 101-114.

Burton, A., Bathurst, J.C., 1998. Physically based modelling of shallow landslide yield at a catchment scale. Environmental Geology 35 (2-3): 89-99.

Chang, J.-C., 1996. Natural hazards in Taiwan. GeoJournal 138 (3): 251-257.

Chang, K.-T., Chiang, S.-H., 2009. An integrated model for predicting rainfall-induced landslides. Geomorphology 105: 366-373.

Chang, K.-T., Chiang, S.-H., Lei, F., 2008. Analysing the Relationship Between Typhoon-Triggered Landslides and Critical Rainfall Conditions. Earth Surface Processes and Landforms 33: 1261-1271.

Chen, C.-Y., Lin, L.-Y., Yu, F.-C., Lee, C.-S., Tseng, C.-C., Wang, A.-H., Cheung, K.-W., 2007. Improving debris flow monitoring in Taiwan by using high-resolution rainfall products from QPESUMS.

Natural Hazards 40 (2): 447-461.

Chen, S.-C., Wu, C.-H., 2007. The evaluation of landslide depth and sediment yield due to typhoon events in Taiwan. Geophysical Research Abstracts 9.

Chen, Y.-G., Liu, T.-K., 2000. Holocene uplift and subsidence along an active tectonic margin: southwestern Taiwan. Quaternary Science Reviews, 19, 923-930.

Chiang, S.-H., Chang, K.-T., 2009. Application of radar data to modeling rainfall-induced landslides. Geomorphology 103: 299-309.

Claessens, L., 2005. Modelling landslide dynamic in forested landscapes. PhD Thesis, Wageningen University, The Netherlands.

Claessens, L., Heuvelink, G.B.M., Schoorl, J.M., Veldkamp, A., 2005. DEM resolution effects on shallow landslide hazard and soil redistribution modelling. Earth Surface Processes and Landforms 30: 461-477.

Claessens, L., Knapen, A., Kitutu, M.G., Poesen, J., Deckers, J.A., 2007b. Modelling landslide hazard, soil redistribution and sediment yield of landslides on the Ugandan footslopes of Mount Elgon. Geomorphology 90: 23–35.

Claessens, L., Schoorl, J.M. and Veldkamp A., 2007a. Modelling the location of shallow landslides and their effects on landscape dynamics in large watersheds: An application for Northern New Zealand. Geomorphology 87, 16–27.

Crosta, G.B., Frattini, P., 2003. Distributed modelling of shallow landslides triggered by intense rainfall. Natural Hazards and Earth System Sciences 3: 81-93.

Crozier, M.J., 1999. Prediction of rainfall-triggered landslides: a test of the antecedent water status model. Earth Surface Processes and Landforms 24: 825-833.

CWB, Central Weather Bureau, Taiwan. www.cwb.gov.tw/V6e/statistics/monthlyData/mD.php, visited on 28-07-2009.

Dadson, S.J., Hovius, N., Chen, H., Dade, W.B., Hsieh, M.-L., Willett, S.D., Hu, J.-C.,Horng, M.-H., Chen, M.-C., Stark, C.P., Lague, D., Lin, J.-C., 2003. Links between erosion, runoff variability and seismicity in the Taiwan orogen. Nature 426: 648-651.

Frattini, P., Crosta, G., Sosio, R., 2009. Approaches for defining thresholds and return periods for rainfall-triggered shallow landslides. Hydrological Processes 23: 1444-1460.

Freer, J., McDonnell, J.J., Beven, K.J., Peters, N.E., Burns, D.A., Hooper, R.P., Aulenbach, B., Kendall, C., 2002. The role of bedrock topography on subsurface storm flow. Water Resources Research 38 (12): 1269.

Garbrecht, J., Martz, L., 1994. Grid size dependency of parameters extracted from digital elevation models. Computers and Geosciences 20: 85-87.

Gertner, G., Wang, G., Fang, S., Anderson, A.B., 2002. Effects and uncertainty of digital elevation model spatial resolutions on predicting the topographical factor for soil loss estimation. Journal of

Soil and Water Conservation 57 (3): 164-174.

Greenway, D.R., 1987. Vegetation and slope stability. In: Anderson, M.G., Richards, K.S. (eds.), Slope stability. Wiley, Chichester, UK, pp. 187-230.

Greenway, D.R., Anderson, M.G., Brian-Boys, K.C., 1984. Influence of vegetation on slope stability in Hong Kong. Proc. 4th Int. Symp. Landslides, Toronto, Canada, vol.1: 399-404.

Hasegawa, S., Dahal, R.K., Nishimura, T., Nonomura, A., Yamanaka, M., 2009. DEM-based analysis of earthquake-induced shallow landslide susceptibility. Geotechnical and Geological Engineering 27 (3): 123-130.

Head, K. H., 1994. Manual of soil laboratory testing, volume 2: permeability, shear strength and compressibility tests, second edition. Pentech Press, London, UK.

Hong, N.M., Chu, H.-J., Lin, Y.-P., Deng, D.-P., 2009. Effects of land cover changes induced by large physical disturbances on hydrological responses in Central Taiwan. Environmental Monitoring and Assessment, in press.

Hovius, N., Stark, C. P., Chu, H. T., Lin, J. C., 2000. Supply and removal of sediment in a landslide dominated mountain belt: Central Range, Taiwan. Journal of Geology 108: 73–89.

Huang, J.C., Kao, S.J., 2006. Optimal estimator for measuring landslide model efficiency. Hydrology and Earth System Sciences 10, 957–965.

Huang, J.C., Kao, S.J., Hsu, M.L., Lin, J.C., 2006. Stochastic procedure to extract and to integrate landslide susceptibility maps: an example of mountainous watershed in Taiwan. Natural Hazards and Earth System Sciences 6: 803–815.

Ibsen, M.-L., Casagli, N., 2004. Rainfall patterns and related landslide incidence in the Porretta-Vergato region, Italy. Landslides 1: 143–150.

Irfan, T.Y., Tang, K.Y., 1992. Effects of the coarse fractions on the shear strength of colluviums. Geotechnical Engineering Office, Hong Kong, Geo Report No. 23, 224 p.

Iverson, R.M., 2000. Landslide triggering by rain infiltration. Water Resources Research 36 (7): 1897-1910.

Keim, R.F., Skaugset, A.E., 2003. Modelling effects of forest canopies on slope stability. Hydrological Processes 17: 1457-1467.

Kuriakose, S.L., Van Beek, L.P.H., Van Westen, C.J., 2009. Parameterizing a physically based shallow landslide model in a data poor region. Earth Surface Processes and Landforms 34: 867-881.

Lee, S., Choi, J., Woo, I., 2004. The effect of spatial resolution on the accuracy of landslide susceptibility mapping: a case study in Boun, Korea. Geosciences Journal 8 (1): 51-60.

Liew, P.M., Pirazzoli, P.A., Hsieh, M.L., Arnold, M., Barusseau, J.P., Fontugne, M., Giresse, P., 1993. Holocene tectonic uplift deduced from elevated shorelines, eastern Coastal Range of Taiwan. Tectonophysics, 222: 55-68.

Malamud, B.D., Turcotte, D.L., Guzzetti, F., Reichenbach, P, 2004. Landslide inventories and their

statistical properties. Earth Surface Processes and Landforms 29: 687-711.

Mejía-Navorra, M., Wohl, E.E., Oaks, S.D., 1994. Geological hazards, vulnerability, and risk assessment using GIS: model for Glenwood Springs, Colorado. Geormorphology 10: 331-354

Montgomery, D.R., Dietrich, W.E., 1994. A physically based model for the topographic control on shallow landsliding. Water Resources Research 30, 1153-1171.

Moore, I.D., O'Loughlin, E.M., Burch, G.J., 1988. A contour based topographic model for hydrological and ecological applications. Earth Surface Processes and Landforms 13, 305-320.

O'Loughlin, E.M., 1986. Prediction of surface saturation zones in natural catchments by topographic analysis. Water Resources Research 22, 794-804.

Pack, R.T., Tarboton, D.G., Goodwin, C.N., 1998. Terrain Stability Mapping with SINMAP, technical description and users guide for version 1.00, Report Number 4114-0, Terratech Consulting Ltd., Salmon Arm, B.C., Canada.

Pack, R.T., Tarboton, D.G., Goodwin, C.N., 2001. Assessing terrain stability in a GIS using SINMAP. 15th annual GIS conference, GIS 2001, Vancouver, British Columbia.

Quinn, P., Beven, K., Chevallier, P., Planchon, O., 1991. The prediction of hillslope flow paths for distributed hydrological modelling using digital terrain models. Hydrological Processes 5, 59-79.

Rahardjo, H., Indrawan, I.G.B., Leong, E.C., Yong, W.K., 2008. Effects of coarse-grained material on hydraulic properties and shear strength of top soil. Engineering Geology 101: 165-173.

Reneau, S.L., Dietrich, W.E., 1987. The importance of hollows in debris flow studies; examples from Marin County, California. In: Costa, J.E., Wieczorek, G.F. (eds). Debris flows/avalanches: process, recognition, and mitigation. Geological Societyof America Reviews in Engineering Geology 7, Geological Society of America, Boulder, Colorado, pp 165–180.

Ritchie, J.C., McHenry, J.R., 1990. Application of radioactive fallout Cesium-137 for measuring soil erosion and sediment accumulation rates and patterns: a review. Journal of Environmental Quality 19: 2, 215-233.

Sakals, M.E., Sidle, R.C., 2004. A spatial and temporal model of root cohesion in forest soils. Canadian Journal of Forest Research 34: 950-958.

Schmidt, K.M., Roering, J.J., Stock, J.D., Dietrich, W.E., Montgomery, D.R., Schaub, T., 2001. The variability of root cohesion as an influence on shallow landslide susceptibility in the Oregon Coast Range. Canadian Geotechnical Journal 38: 995-1024.

Schoorl, J.M., Sonneveld, M.P.W., Veldkamp, A., 2000. Three-dimensional landscape process modelling: the effect of DEM resolution. Earth Surface Processes and Landforms 25: 1025-1043.

Selby, M., 1993. Hillslope materials and processes. Oxford University Press, Oxford, US.

Sidle, R.C., Pearce, A.J., O'Loughlin, C.L., 1985. Hillslope stability and land use. Water Resources Monograph 11. American Geophysical Union, Washington DC, 312 pp.

Tarolli, P., Tarboton, D.G., A new method for determintation of most likely landslide initiation

points and the evaluation of digital terrain model scale in terrain stability mapping. Hydrology and Earth System Sciences 10: 663-677.

Tian, Y., X, C.-C., Liu, Y., Wu, L., 2008. Effects of raster resolution on landslide susceptibility mapping: A case study of Shenzhen. Science in China Series E: Technological Sciences 51, Supp. II: 188-198.

Tsai, C.-C., Chen, Z.-S., Duh, C.-T., Horng, F.-W., 2001. Prediction of soil depth using a soil-landscape regression model: A case study on forest soils in southern Taiwan. Proceedings of the National Science Council, R.O.C., Vol. 25, No. 1. pp 34-39.

Tsai, T.-L., The influence of rainstorm pattern on shallow landslide. Environmental Geology 53: 1563-1569.

Uchida, T., Tamura, K., Mori, N., 2008. A simple method for producing probabilistic shallow landslide hazard maps using soil thickness dataset. Geophysical Research Abstracts, Vol. 10, European Geosciences Union.

Van Beek, L.P.H., Van Asch, Th.W.J., 2004. Regional Assessment of the Effects of Land-Use Change on Landslide Hazard by Means of Physically Based Modelling. Natural Hazards 31: 289-304.

Wilson, J.P., Repetto, P.L., Snyder, R.D., 2000. Effect of data source, grid resolution and flow-routing method on computed topographic attributes. In: Wilson, J.P., Gallant, J.C. (eds), Terrain Analysis: Principles and Applications. John Wiley & Sons, Chichester, UK, pp. 139-164.